Modeling vascular diseases using human induced pluripotent stem cells

Cao, X.

Chapter 6

Pseudomyogenic hemangioendothelioma recapitulated in endothelial cells from human induced pluripotent stem cells engineered to express the *SERPINE1-FOSB* translocation

David G.P. van IJzendoorn[1], Daniela C.F. Salvatori[2,6#], Xu Cao[3#], Francijna van den Hil[3], Inge H. Briaire-de Bruijn[1], Danielle de Jong[4], Hailiang Mei[5], Christine L. Mummery[3], Karoly Szuhai[4], Judith V.M.G. Bovée[1*], Valeria V. Orlova[3*]

[1]Department of Pathology, Leiden University Medical Center, Leiden, The Netherlands
[2]Central Laboratory Animal Facility, Leiden University Medical Center, Leiden, The Netherlands; 6Department of Pathobiology, Anatomy and Physiology Division, Faculty of Veterinary Medicine, Utrecht University, Utrecht, The Netherlands.
[3]Department of Anatomy and Embryology, Leiden University Medical Center, Leiden, The Netherlands
[4]Department of Cell and Chemical Biology, Leiden University Medical Center, Leiden, The Netherlands
[5]Sequencing analysis support core, Leiden University Medical Center, Leiden, The Netherlands

[#]Contributed equally
[*]Contributed equally, Correspondence: v.orlova@lumc.nl and J.V.M.G.Bovee@lumc.nl

Data submitted in part to Cell Reports Medicine;
Extended data in **Chapter 6 Appendix**: Follow up bioinformatics analysis of hiPSC-endothelial cells expressing the SERPINE1-FOSB translocation

ABSTRACT

Chromosomal translocations are prevalent among soft tissue tumors including those of the vasculature. Pseudomyogenic hemangioendothelioma (PHE) is one such tumor. It has features of endothelial cells (ECs) and a tumor-specific t(7;19)(q22;q13) *SERPINE1-FOSB* translocation, but has been difficult to study since to date no cell lines have been derived from the tumor. To address this, we engineered the PHE chromosomal translocation into human induced pluripotent stem cells (hiPSCs) using CRISPR/Cas9 and differentiated these into ECs (hiPSC-ECs). Comparison of parental and modified (PHE) lines with the t(7;19)(q22;q13) *SERPINE1-FOSB* translocation showed (i) elevated expression of *FOSB* specifically in hiPSC-ECs *in vitro* and *in vivo* (ii) increased proliferation and tube formation but decreased endothelial barrier function (iii) invasive growth and abnormal vessel formation in mouse after transplantation of the mutated cells (iv) transcriptome alterations specific for hiPSC-ECs that reflect the PHE phenotype and elucidate pathways regulated by the fusion that can be targeted for treatment (PI3K-Akt and MAPK signaling). hiPSC-ECs carrying the *SERPINE1-FOSB* translocation thus recapitulated functional features of PHE and demonstrated that this approach can yield models of translocation-driven tumors for identification of therapeutic targets and deeper understanding of underlying tumorigenic mechanisms.

INTRODUCTION

Chromosomal translocations and their corresponding gene fusions are common in neoplasia and are important in the initiation of tumorigenesis (Mitelman et al., 2007). These gene fusions are especially prevalent in soft tissue tumors, of which ~15-20% carry a recurrent chromosomal translocation with no, or few, additional genomic alterations (Mertens et al., 2016). Moreover, translocations are usually specific for each subtype. The identification of specific fusion genes has significantly increased the understanding of the pathogenesis of these (often-rare) tumor types and are used as an auxiliary diagnostic tool.

Pseudomyogenic hemangioendothelioma (PHE) is a rare soft tissue tumor characterized by a specific recurrent balanced translocation, t(7;19)(q22;q13), which fuses SERPINE1 to FOSB (Trombetta et al., 2011; Walther et al., 2014). The translocation leads to the loss of the first exon of FOSB containing the start codon, resulting in a novel start codon in exon 2 of FOSB. The translocation therefore causes loss of 48 amino acids at the start of the FOSB protein which then falls consequently under control of the SERPINE1 promoter (Walther et al., 2014). PHE is locally aggressive, rarely metastasizing and often affecting young adults, especially men between 20-50 years of age. The disease most often presents as multiple discontiguous lesions in different tissue planes (Hornick and Fletcher, 2011). Approximately 60% of the

patients show relapse after surgical removal or develop additional nodules which can necessitate limb amputation. The tumors display loose spindle-shaped cells with abundant eosinophilic cytoplasm, that invade in the surrounding soft tissues, expressing vascular (CD31, ERG) and epithelial (keratin) markers. Moreover, the translocation results in overexpression of FOSB protein in patient tumor samples (Hung et al., 2017). Although PHE does not form functional blood vessels, vascular markers are expressed suggesting that PHE arises from endothelial cells (ECs) or their precursors. The tumor is therefore classified among the group of vascular tumors (Billings et al., 2003; Hornick and Fletcher, 2011; Ide et al., 2015).

Further understanding of the underlying molecular mechanisms is required to rationally design systemic therapy for patients with inoperable disease. However, like many other soft tissue tumors with translocations, PHE is rare and no cell lines have yet been derived from the tumor, confounding understanding of tumorigenesis and the identification of potential therapeutic targets. A possible approach to model translocation driven tumors is to engineer the complete chromosomal translocation in human pluripotent stem cells and examine the effects on appropriately differentiated derivatives (Sánchez-Rivera and Jacks, 2015). Engineered nucleases were recently shown to be useful in generating chromosomal translocations in human cells. Clustered regularly interspaced short palindromic repeats (CRISPR) and Cas9 nucleases have been used to introduce chromosomal translocations in human umbilical cord-derived mesenchymal stromal cells (hMSCs), umbilical cord blood-derived CD34+ cells, and more recently human induced pluripotent stem cells (hiPSCs) (Schneidawind et al., 2018; Torres et al., 2014; Torres-Ruiz et al., 2017; Vanoli et al., 2017). hiPSCs in particular are increasingly used as human disease models, as they can be propagated indefinitely *in vitro* and differentiated into most cell types of the body (Takahashi et al., 2007), including ECs (Halaidych et al., 2018a; Orlova et al., 2014a; 2014b). They are thus a renewable source of cells to study human physiology and disease. We hypothesized that hiPSC-derived ECs (hiPSC-ECs) could be valuable for modeling rare tumors such as those of the vasculature and demonstrated in the study described here that this is indeed the case for PHE.

We introduced the t(7;19)(q22;q13) *SERPINE1-FOSB* translocation into hiPSCs and thus generated control and modified isogenic hiPSC pairs. We carried out functional analysis of hiPSC-ECs and whole genome and transcriptome sequencing of isogenic pairs of hiPSC and hiPSC-EC with and without translocation. We showed that hiPSC-ECs with the *SERPINE1-FOSB* fusion were distinct from their isogenic controls and exhibited phenotypic and transcriptomic characteristics very similar to PHE. More importantly, in mice mutant hiPSC-ECs became invasive and formed abnormal vessels. Our hiPSC model thus mimics PHE, but in more general terms, the approach can serve as a blueprint for using CRISPR/Cas9 in hiPSCs to explore the role of fusion genes in the

development of specific rare cancer subtypes for which cell lines are lacking, providing deeper understanding of tumorigenesis resulting from gene fusions.

RESULTS

Introduction of t(7;19)(q22;q13) *SERPINE1-FOSB* translocation in hiPSCs

We used CRISPR/Cas9-facilitated gene targeting to introduce the t(7;19)(q22;q13) translocation in hiPSCs. We generated a fusion between intron 1 of SERPINE1 and intron 1 of FOSB, which leads to the same novel start codon as found in PHE tumors from patients (figure 1a). Two double stranded DNA breaks were introduced in the genome guided by two gRNAs targeting SERPINE1 intron 1 and FOSB intron 1. A repair template was provided for homologous directed recombination (HDR) containing two 1000 bp homology arms for SERPINE1 and FOSB, separated by an excisable neomycin resistance cassette flanked by Flp-recombinase sequences (FRT) (figure 1a). A wild-type hiPSC line generated from an anonymous "healthy" donor using non-integrating Sendai virus (SeV) was used for targeting (Halaidych et al., 2018a). hiPSCs were simultaneously transfected with vectors containing Cas9, gRNAs and HDR template (schematic overview of the targeting strategy in hiPSCs is shown in supplementary figure 1a). Neomycin selection allowed enrichment of hiPSCs with integration of the targeting template. The neomycin cassette was next removed by transient transfection of Flp-recombinase. Three color fluorescence in situ hybridization (FISH) revealed that translocations occurred relatively frequently, with 20 of 100 screened cells harboring a split of the FOSB bracketing probes (chromosome 19) and a colocalization of the distal FOSB probe to the SERPINE1 (chromosome 7) (supplementary figure 1b). hiPSC clones derived from single cells were screened by PCR and the presence of the SERPINE1-FOSB gene fusion was confirmed in 2 out of 73 (2.7% of targeted cells, clones D3 and G6) (figure 1b). Sanger sequencing of PCR products confirmed the correct translocation (figure 1a and supplementary figure 2a). This shows that although translocations between chromosomes 7 and 19 were relatively common events (20% of targeted cells showed translocation detected by FISH), most of these translocations likely occur via non-homologous end joining (NHEJ) and possibly contain large deletions/insertions. They were therefore not detected during PCR screening, resulting in only 2 correctly targeted clones (2.7% targeting efficiency). The targeted allele of hiPSC clone D3 was found to have an FRT remaining between SERPINE1 and FOSB as expected (figure 1a), while this insert was absent in the targeted allele of hiPSC clone G6 due to the translocation occurring via NHEJ (supplementary figure 2a). The non-targeted wild-type alleles of SERPINE1 and FOSB were also Sanger sequenced. In clone D3 a single nucleotide insertion was found in both the non-targeted wild-type SERPINE1 intron 1 and the non-targeted wild-type FOSB intron 1 (supplementary figure 2b, c). In clone G6, a 9 base-pair deletion was found in the non-targeted wild-type FOSB intron 1 (supplementary figure 2b). In addition, clone G6

contained an insertion of ~1220 bp of the repair template in the non-targeted wild-type SERPINE1 intron 1, which was evident on the DNA gel and Sanger sequencing (figure 1b and supplementary figure 2c). Analysis of the corresponding cDNA showed presence of fused SERPINE1 5' UTR and FOSB exon 2 in both clones D3 and G6 (supplementary figure 2d) identical to that found in PHE patients, and the presence of correctly spliced wild-type SERPINE1 (supplementary figure 2e). Neither clone D3 or G6 had karyotypic abnormalities, other than the balanced t(7;19)(q22;q13) translocation, as seen using COmbined Binary RAtio Labeling Fluorescence in Situ Hybridization (COBRA-FISH) (figure 1c).

To verify that the targeting with CRISPR/Cas9 did not result in deleterious off-target effects, whole-genome sequencing was performed. No additional copy number variations, insertions or deletions, structural variants or single nucleotide variants (SNVs) were found in the coding genome of the targeted hiPSC clones D3 and G6 (hiPSCSERPINE1^{-FOSB}) compared to the parental control hiPSCs (hiPSC^{WT}) (figure 1d). Furthermore, the *in silico* predicted off target sites for the guide-RNAs used showed no additional alterations (synonymous or non-synonymous) compared with the untargeted parental control hiPSCs (figure 1d).

To verify pluripotency of the targeted and parental control hiPSC lines, teratoma assay was performed in mice. Targeted and parental control hiPSCs retained the ability to form tissues derived from all three germ layers (endoderm, mesoderm and ectoderm), showing that CRISPR-Cas9 targeting has not affected pluripotency (figure 1e).

Differentiation and characterization of ECs from hiPSC^{WT} and hiPSC$^{SERPINE1\text{-}FOSB}$ lines

hiPSCs with and without *SERPINE1-FOSB* fusion were differentiated into ECs using a protocol previously described (Halaidych et al., 2018a; Orlova et al., 2014b; 2014a) (figure 2a). hiPSC-ECs were purified on day 10 of differentiation by CD31^{+} cell selection, expanded and cryopreserved for further characterization. hiPSC-ECsWT and hiPSC-ECsSERPINE1-FOSB differentiated from two targeted clones (D3 and G6) exhibited typical EC morphology (figure 2b and data not shown) and showed cell surface expression of known EC markers, such as vascular endothelial (VE)-cadherin (VEC), CD31, CD34, VEGFR2, VEGFR3 and CD105, as expected and in accordance with our previous findings (Orlova et al., 2014a) (figure 2c,d and supplementary figure 3a,b). Interestingly, hiPSC-ECs derived from both the D3 and G6 targeted clones displayed increased expression of CD105 (figure 2d and supplementary figure 3b), which is known to be upregulated in tumor endothelial cells (Miller et al., 1999) as well as in vascular tumors (Verbeke et al., 2013). Moreover, expression of FOSB mRNA showed a 4.9 log2 fold increase in hiPSC-ECs from clone D3 and a 5.9 log2 fold increase in hiPSC-ECs from clone G6 compared to the isogenic hiPSC-ECs derived from parental non-targeted hiPSC line (figure 2e and supplementary figure 3c). The increase in *FOSB* expression at the mRNA

level was also evident as an increase in protein expression by Western blot, where FOSB was detected in hiPSC-ECs$^{SERPINE1\text{-}FOSB}$ but not in hiPSC-ECs^{WT} (figure 2f and supplementary figure 3d).

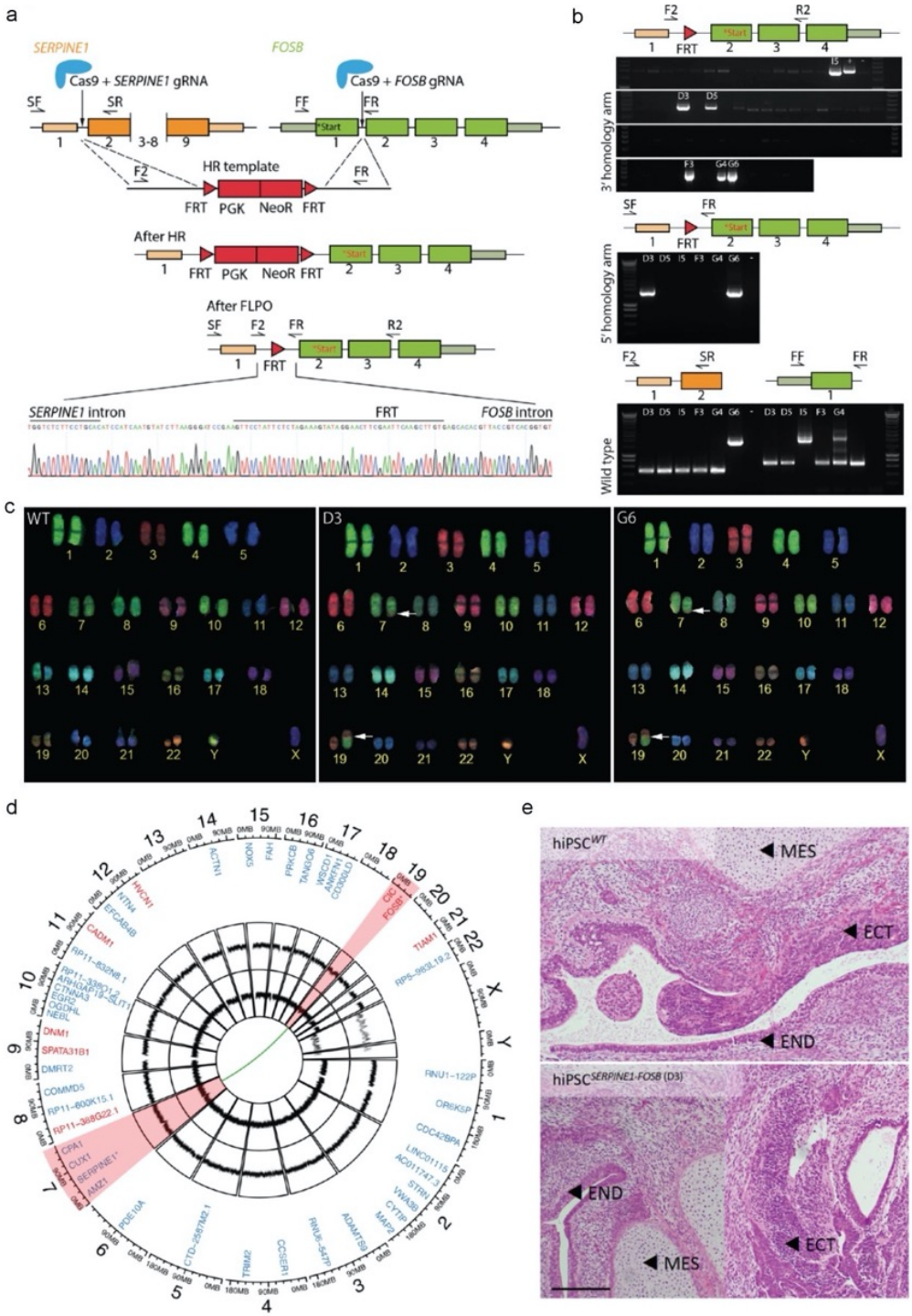

Figure 1. **Generation and characterization of hiPSCs with a *SERPINE-FOSB* fusion. (a)** Schematic overview of the targeting strategy for generation of a *SERPINE1-FOSB* gene fusion. Filled boxes are exons, lines introns. FOSB start codons are labeled in the figure, in black text represents the original start codon while the new start codon after the fusion is shown in red. Two double stranded breaks were introduced in the genome guided by two gRNAs in SERPINE1 intron 1 and FOSB intron 1. A repair template used for homologous recombination (HR template) with neomycin resistance cassette flanked by Flp-recombinase sequences (FRT), as well targeted genomic locus prior (After HR) and after FLP-mediated neomycin removal (after FLPO). Bottom panel shows Sanger sequencing of PCR products from the clone with translocation validating HDR recombination of SERPINE1 and FOSB with remaining FRT sequence left from the repair template (D3 clone). (b) Representative results of PCR screen on single cell-derived hiPSC clones using primers (F2, R2 and SF, SR; F2, SR and FF and FR) shown in panel above the PCR screen results. Two targeted clones (D3 and G6) were identified out of 73 screened clones. PCR shows clone G6 has a large insert in the *SERPINE1* wild-type allele. **(c)** COBRA-FISH on colony metaphase cells of WT, D3 and G6 hiPSC clones shows a balanced translocation t(7;19)(q22;q13); furthermore no additional chromosomal abnormalities were evident in any of the screened cells. **(d)** Whole genome sequencing was performed and the results are summarized in a Circos plot. The first layer shows all genes that are potential off-target sites for the gRNA for *FOSB* (red) and *SERPINE1* (blue). No mutations were found in the off-target sites and the surrounding 100 bases. The second and third layers show Copy Number Analysis (CNA) for clones D3 and G6 respectively compared to the isogenic control. No Copy Number Variations (CNVs) are detected. The green connection line shows the detected *SERPINE1-FOSB* fusion, as detected in both clones D3 and G6. Chromosomes 7 and 19, involved in the translocation, are highlighted in red. **(e)** Teratoma formation in mice. Top panel shows teratomas formed from the hiPSC^{WT}, the bottom panel from the hiPSC$^{SERPINE1\text{-}FOSB\ (D3)}$; two sections of each are shown. Cellular derivatives of the three germ lineages are indicated: mesoderm (MES), ectoderm (ECT) and endoderm (END). Scale bar indicates 200 μm.

Functionality of ECs from hiPSC^{WT} and hiPSC$^{SERPINE1\text{-}FOSB}$ lines

To investigate the effect of the *SERPINE1-FOSB* fusion on hiPSC-ECs functionality, we next performed assessment of proliferation and Matrigel tube formation assay. *SERPINE1-FOSB* fusion caused increased EC proliferation. The effect measured after 24 hours was most prominent in basal EC growth medium supplemented with 1% platelet-poor serum (PPS) (1.9-fold increase), followed by basal EC growth medium supplemented with both 1% PPS and VEGF (1.58 vs 2.27-fold) (figure 2g). No significant differences in EC proliferation were observed using complete EC growth medium (full) that in addition to VEGF also contained bFGF, indicating that FOSB overexpression

caused by the *SERPINE1-FOSB* fusion may result in a VEGF-independent growth advantage for ECs. Matrigel tube formation assays showed significant increase in number of junctions (147 vs 218, p<0.001) and meshes (53 vs 85, p<0.005) in hiPSC-ECs $^{SERPINE1\text{-}FOSB}$ compared to isogenic control hiPSCs-ECs^{WT} after 48 hours (figure 2h).

Barrier function of ECs from hiPSC^{WT} and hiPSC$^{SERPINE1\text{-}FOSB}$ lines

Barrier function of hiPSC-ECs with and without the *SERPINE1-FOSB* fusion was next examined by real-time impedance spectroscopy with an integrated assay of electric wound healing, as demonstrated previously (Halaidych et al., 2018a). The *SERPINE1-FOSB* fusion resulted in a significant decrease in barrier function of hiPSC-ECs (figure 3a, b and supplementary figure 4a,b). Barrier function depends on the integrity of cell junction complexes that form tight- and adherence junctions. Therefore, we also investigated junctional integrity in hiPSC-ECs with *SERPINE1-FOSB* fusion using the tight junctional marker *zonula occludens* (ZO)-1, the adherence junctional marker VEC and counterstained for F-actin and CD31 (figure 3c, d). Presence of less organized, "zig-zag" patterns of ZO1 and VEC was evident for hiPSC-ECs$^{SERPINE1\text{-}FOSB}$ compared to the hiPSC-ECs^{WT} (figure 3c, d), which is in line with reduced barrier function of hiPSC-ECs with *SERPINE1-FOSB* fusion.

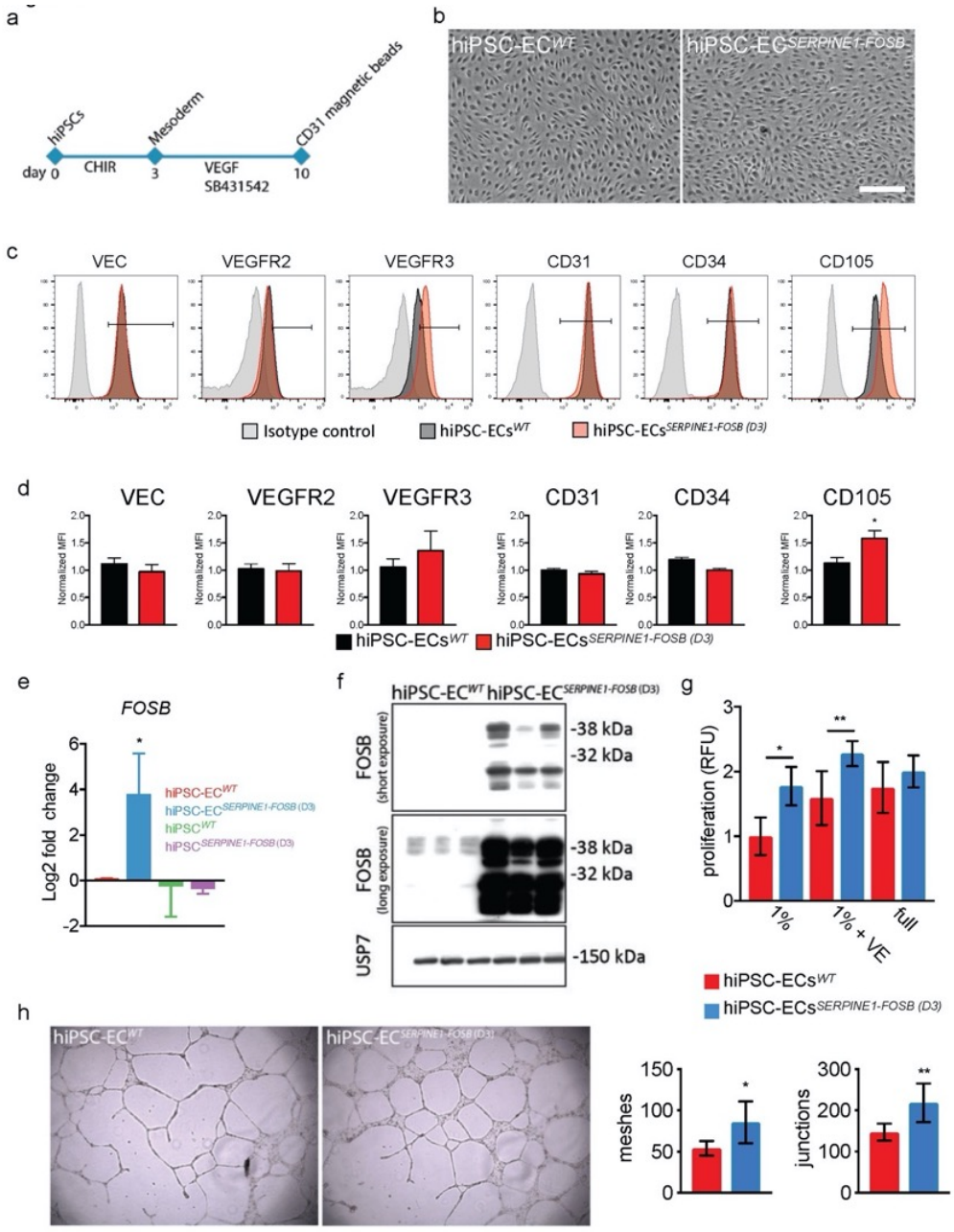

Figure 2. Differentiation and characterization of hiPSC-ECs with *SERPINE1-FOSB* fusion. (a) Schematic overview of the differentiation protocol and purification of ECs from hiPSCs. **(b)** Bright field images showing typical EC morphology of hiPSC-ECs. Scale bar represents 500 μm. **(c)** FACS analysis of EC markers expression on isolated ECs at passage 3 (P3) from hiPSC-ECs^{WT} (black filled histogram) and hiPSC-ECs$^{SERPINE1\text{-}FOSB}$ (D3) (red filled histogram), and relevant isotype control (gray filled histogram). (d) Quantification of normalized relative surface expression levels (MFI) of VEC, VEGFR2, VEGFR3, CD31, CD34 and CD105. Error bars are SD, * p<0.005. (e) Real-time qPCR analysis of FOSB expression in hiPSCs^{WT}, hiPSCs$^{SERPINE1\text{-}FOSB}$ (D3), hiPSC-ECs^{WT} and hiPSC-$^{ECsSERPINE1\text{-}}$

FOSB (D3). Expression is determined relative to hiPSC-ECs^{WT}, shown as log2 fold change. Error bars are SD, * p<0.05. (f) Western blot of FOSB expression in hiPSC-ECs^{WT} and hiPSC-ECs$^{SERPINE1\text{-}FOSB}$ (D3). Short and long exposure of the gel is shown. USP7 was used as a housekeeping control. (g) Analysis of hiPSC-ECs^{WT} and hiPSC-ECs$^{SERPINE1\text{-}FOSB}$ (D3) proliferation rates when cultured in basal endothelial cell growth medium supplemented with 1%PPS (1%), 1%PPS supplemented with 50 ng/ml VEGF (1% VE) or complete EC growth medium (full) for 24 hours. Proliferation was determined by using a Presto Blue assay. Error bars are shown as SD, * p<0.0001, ** p<0.0005. **(h)** Representative images of Matrigel tube formation assay using hiPSC-ECs^{WT} and hiPSC-ECs$^{SERPINE1\text{-}FOSB\ (D3)}$ at the 48h time point. Right panel shows quantification of the number of junctions and meshes. Error bars are SD, * p<0.005, ** p<0.001. All experiments were performed in triplicate using three independent batches of hiPSC-ECs.

Functionality of hiPSC-ECs from hiPSC^{WT} and hiPSC$^{SERPINE1\text{-}FOSB}$ lines *in vivo* in mice

In order to test the functionality and the ability to form functional perfused blood vessels, hiPSC-ECs with and without *SERPINE-FOSB* translocation were injected in mice in a Matrigel Plug Assay that allows assessment of vasculogenesis, as described previously (Halaidych et al., 2018). Matrigel plugs were excised and analyzed 4- and 16-weeks post-transplantation. Both hiPSC-ECsWT and hiPSC-ECs$^{SERPINE1\text{-}FOSB}$ (D3) formed stable vessels in vivo composed of human ECs evident at the 4-weeks (figure 4a) and 16-weeks post-transplantation (figure 4c). Quantification of the vessel density showed comparable areas covered by human vessels, demonstrating that both hiPSC-ECs^{WT} and hiPSC-ECs$^{SERPINE1\text{-}FOSB}$ (D3) had similar abilities to form vessels *in vivo* (figure 4b, d). The vessels were perfused (as indicated by the presence of red blood cells) (figure 4a, c). Moreover, FOSB positive ECs were evident in the Matrigel plugs with hiPSC-ECs$^{SERPINE1\text{-}FOSB}$ (D3), but not the Matrigel plugs with hiPSC-ECs^{WT} (figure 4e). Furthermore, FOSB positive hiPSC-ECs$^{SERPINE1\text{-}FOSB}$ (D3) also invaded the surrounding mouse soft tissues (the striated muscle) at 16-weeks post-transplantation in two of the three mice whereas this was not observed in any of the mice with hiPSC-ECs^{WT} transplants (figure f, g and h).

The hiPSC-ECsS$^{ERPINE1\text{-}FOSB}$ (D3) vessels at 16 weeks were disorganized and disarrayed and often contained thrombi (conglomeration of fibrin and platelets, containing red blood cells) (figure 4h, i). Thrombi were quantified using phosphotungstic acid-haematoxylin (PTAH) staining (thrombus positive vessels 20.67 vs 81.33 counted in 5.7 mm2, n=3, p=0.1) (figure 5j).

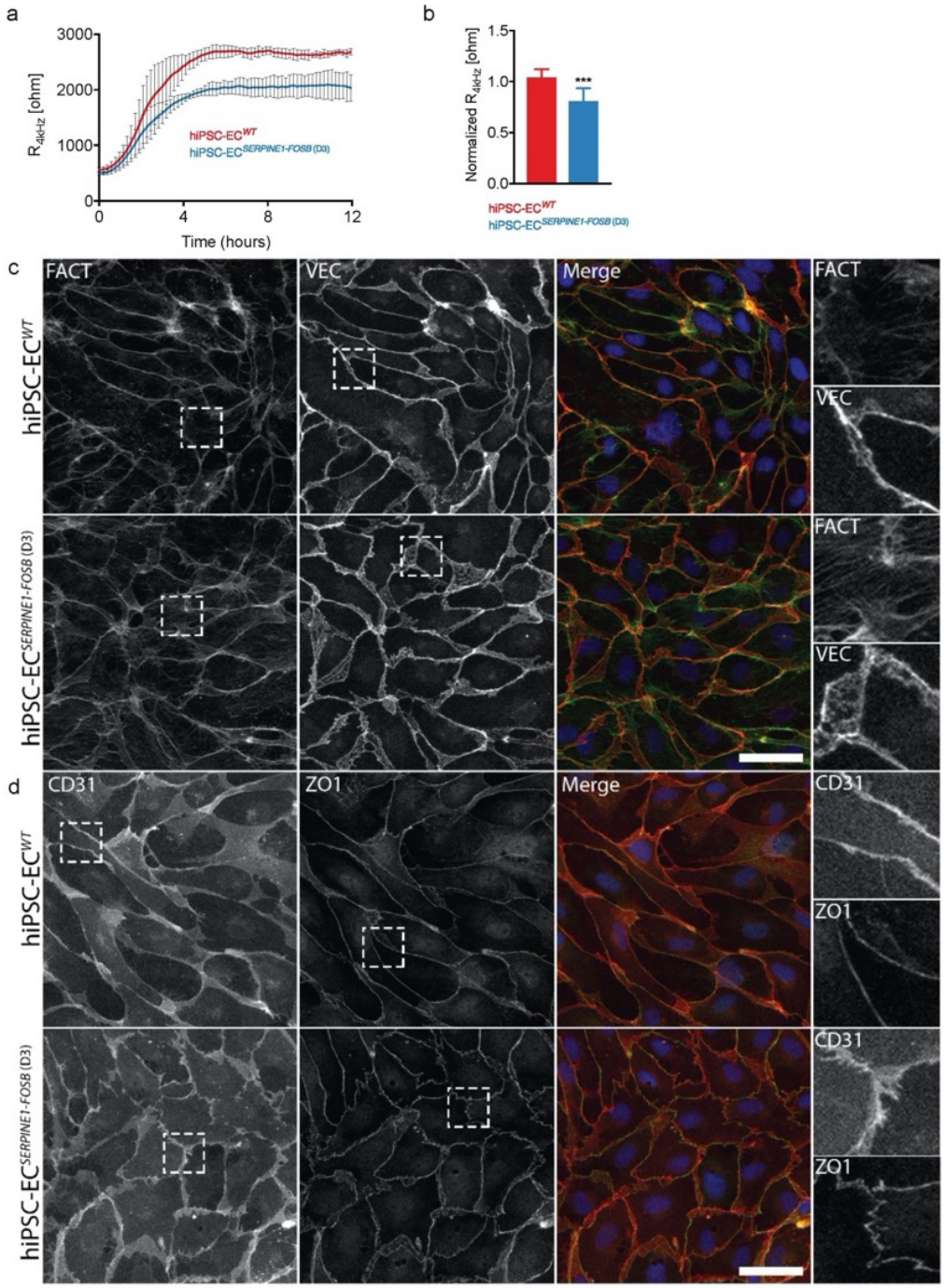

Figure 3. Assessment of barrier function of hiPSC-ECs with *SERPINE1-FOSB* fusion.

(a) Representative absolute resistance of the EC monolayer in complete EC growth medium. Errors bars are shown as ±SD. **(b)** Normalized resistance [4 kHz] of the EC monolayer in complete EC growth medium. Error bars are shown as ±SD of six independent biological experiments. *** p<0.001. **(c, d)** Representative immunofluorescent images of FACT, VEC **(c)** and CD31, ZO1 **(d)** to

analyze the cell adherence and tight junctions. Merged images show FACT in green, VEC in red and DAPI in blue **(c)** and CD31 in red, ZO1 in green and DAPI in blue **(d)**. The right panels show further enlarged areas selected from the shown images (dashed squares). Scale bar represents 50 μm. Experiments were performed in triplicate using three independent batches of hiPSC-ECs.

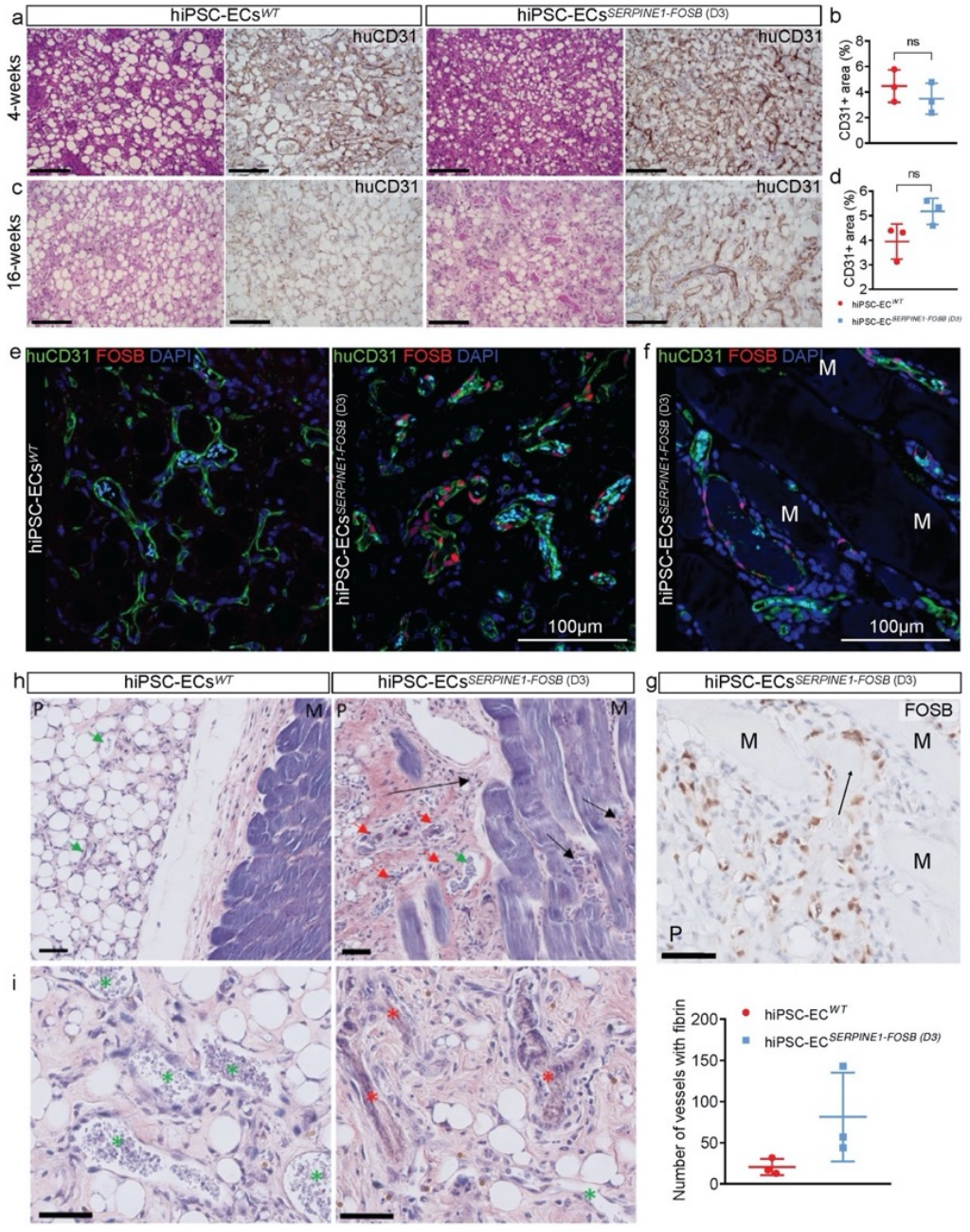

Figure 4. *In vivo* vasculogenesis assay for hiPSC-ECs^{WT} and hiPSC-ECs$^{SERPINE1\text{-}FOSB\ (D3)}$. (a, c) H&E and human CD31 staining of FFPE tissue from the Matrigel plug harvested after 4- (shown in

panel **(a))** and 16- (shown in panel **(c)**) weeks. Both hiPSC^{WT} and hiPSC$^{SERPINE\text{-}FOSB\ (D3)}$ show vessel formation. Scale bar indicates 100 µm. **(b, d)** Vessel density was estimated by quantification of the human CD31^{+} area at 4- and 16-weeks. The 4- and 16-week timepoints showed no significant difference in human CD31^{+} area. **(e, f)** Double immunofluorescent staining with FOSB and human CD31 antibodies counterstained with DAPI on cryosections from Matrigel plug containing hiPSC-ECs^{WT} and hiPSC-ECs$^{SERPINE\text{-}FOSB\ (D3)}$. FOSB is shown in red, CD31 in green and DAPI is blue. The left panel shows the hiPSC-ECs^{WT} experiment, the right panel the hiPSC-ECs$^{SERPINE\text{-}FOSB\ (D3)}$ experiment. Cyan colored objects are representing erythrocytes fluorescing in multiple detection channels. Panels **(f, g)** show invasion of FOSB positive hiPSC-ECs$^{SERPINE1\text{-}FOSB}$ (D3) into the striated muscle at 16-weeks post-transplantation. (g) FOSB IHC on FFPE tissue from Matrigel plug with hiPSC$^{SERPINE1\text{-}FOSB}$ (D30) ECs. Scale bar 50 µm. Surrounding mouse muscle (indicated by M) and the matrigel plug (indicated by P). (**h, i**) PTAH stained sections from the in vivo vasculogenesis assay. hiPSC-ECs^{WT} (left panel) and hiPSC-ECs$^{SERPINE1\text{-}FOSB}$ (D3) (right panel) are shown. Both images show the surrounding mouse muscle (indicated by M) and the Matrigel plug (indicated by a P). Vessels with and without thrombi are indicated by red and green arrows, respectively (h) and red and green stars (i). The black arrows indicate areas with infiltration in the mouse muscle. The scale bar indicates 50 µm. **(j)** Quantification of vessels containing PTAH positive thrombi in hiPSC-ECs^{WT} and hiPSC-ECs$^{SERPINE\text{-}FOSB\ (D3)}$, in an area of 5.7 mm^2, n=3 and p=0.1.

Transcriptome analysis of ECs from hiPSC^{WT} and hiPSC$^{SERPINE1\text{-}FOSB}$ lines

The transcriptomes of hiPSC-ECs with and without SERPINE1-FOSB fusion were compared. 630 and 592 differentially expressed genes (DEGs)(PFDR≤0.05) were upregulated and downregulated respectively in hiPSC-ECs$^{SERPINE1\text{-}FOSB}$ compared to hiPSC-ECs^{WT} (figure 5a). Both FOSB and SERPINE1 were significantly upregulated in hiPSC-ECs$^{SERPINE1\text{-}FOSB}$ compared to hiPSC-ECs^{WT}. Enrichment analysis using the KEGGs (Kyoto Encyclopedia of Genes and Genomes) pathway database revealed several signaling pathways significantly enriched in DEGs upregulated in hiPSC-ECs$^{SERPINE1\text{-}FOSB}$. These included focal adhesion, ECM-receptor interaction, Pathways in cancer, PI3K-Akt, MAPK, TGF-beta and HIF-1 signaling pathways, and Glycolysis/Gluconeogenesis (figure 5b and supplementary figure 5). Upregulation of glycolytic genes in hiPSC-ECs$^{SERPINE1\text{-}FOSB}$ (supplementary figure 5h) indicates possible changes in the metabolic state of ECs, as previously demonstrated for tumor ECs (Cantelmo et al., 2016). No signaling pathways were significantly enriched in DEGs upregulated in hiPSC-EC^{WT}. Gene Ontology (GO) enrichment analysis revealed alterations in the following biological processes in hiPSC-ECs$^{SERPINE1\text{-}FOSB}$: extracellular matrix organization, angiogenesis, cell-matrix adhesion, inflammatory response, cell junction organization, regulation of TGF-beta receptor signaling pathway and others (figure 5c). By contrast, response to interferon-gamma

was the only biological process significantly enriched in DEGs upregulated in hiPSC-EC^{WT} (figure 5c). To demonstrate the relationship between the genes and identified GOs, a gene network map was next constructed using DEGs upregulated in hiPSC-ECs$^{SERPINE1\text{-}FOSB}$ (total of 182 genes) (figure 5d). Gene interaction analysis was next performed using Ingenuity pathway analysis (IPA). Gene interaction networks related to cancer, cellular movement and growth, and TGF-β signaling pathway were used to demonstrate interaction between the identified dysregulated genes and FOSB in hiPSC-ECs$^{SERPINE1\text{-}FOSB}$ (figure 5e). FOSB regulates SERPINE1 directly, which is in line with our previous finding that truncated FOSB was able to regulate its own transcription (van IJzendoorn et al., 2018), as well as via SMAD3. Both exhibit a self-regulatory mechanism, which could further activate many genes in the network of cellular growth and proliferation and cancer processes directly or indirectly through activation of the TGF-β signaling pathway (figure 5e).

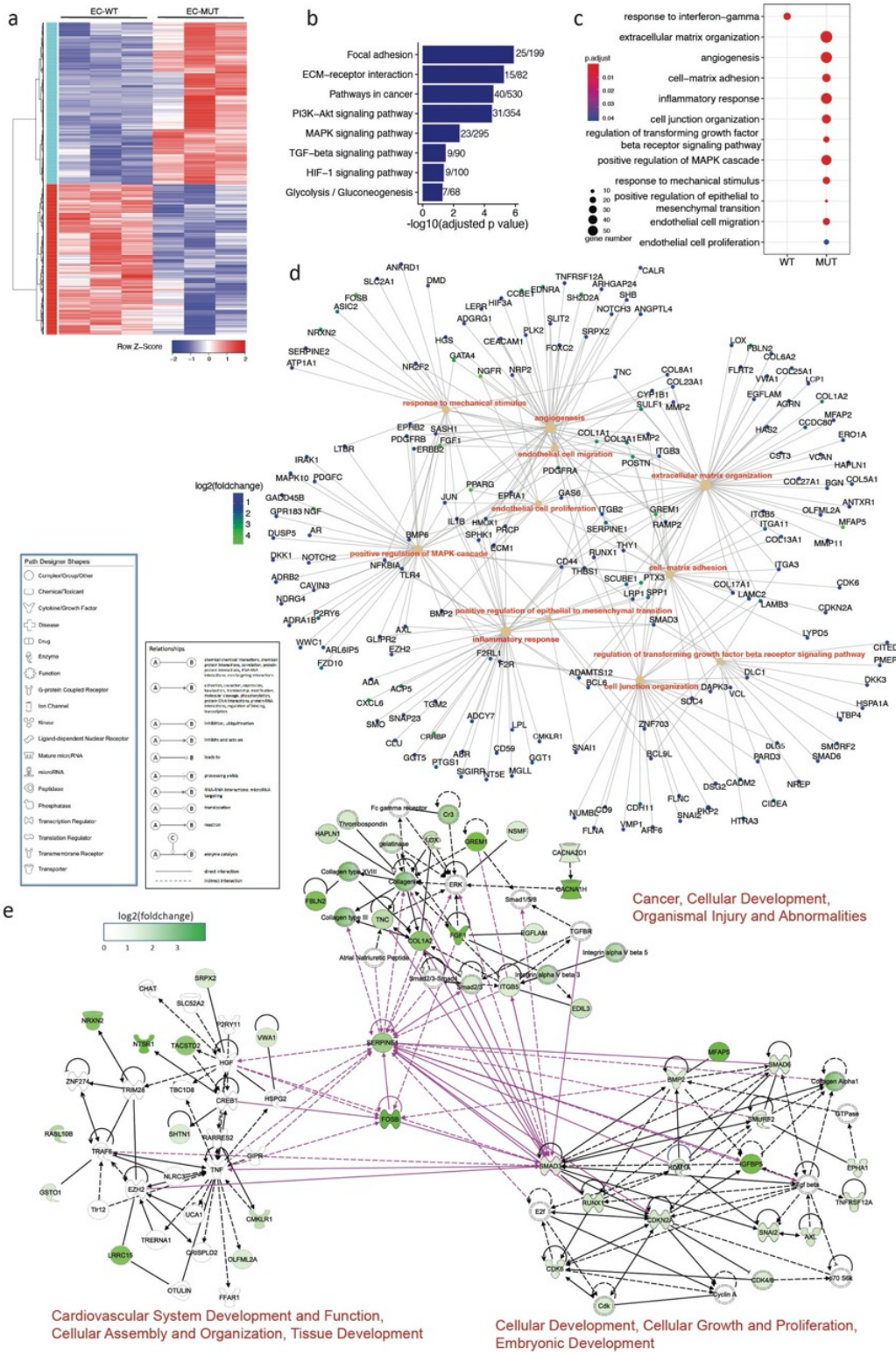

Figure 5. Transcriptome analysis of hiPSC-ECs with and without SERPINE1-FOSB translocation.

(a) Hierarchical clustering analysis (HCA) of differentially expressed genes (DEGs) between hiPSC-ECs^{WT} (WT) and hiPSC-ECs$^{SERPINE1\text{-}FOSB}$ (D3) (MUT) samples (three independent differentiations and isolation for each clone). 630 and 592 significantly upregulated and downregulated genes in MUT were identified compared to WT ECs (PFDR≤0.05). (b) Representative KEGG pathways enriched in upregulated DEGs in MUT ECs (-log10(adjusted p value)) and number of enriched genes within total genes of each pathway are shown. (c) Representative Gene ontologies (GOs) that enriched in downregulated (WT) and upregulated (MUT) DEGs. Size and color indicate gene number and adjusted p value of each GO. (d) Cnetplot of genes associated with enriched GOs (c), color indicates the log2(fold change) of gene expression in MUT compared to WT. (e) Gene interaction network constructed using all genes shown in (c) with Ingenuity pathway analysis (IPA). SERPINE1, FOSB were added manually. Interactions among FOSB and TGF-β signaling pathway and two networks were generated using IPA. Color indicates the log2(fold change) of gene expression in MUT compared to WT.

DISCUSSION

There is an urgent need for *in vitro* models to study rare translocation-driven tumors, both to identify the functional consequences of the translocation, and to identify potential therapeutic targets. We used CRISPR/Cas9 to induce a tumor-associated translocation in hiPSCs, specifically the *SERPINE1-FOSB* translocation to model the rare vascular tumor PHE. Two hiPSC clones among 73 clones screened contained the translocation. In one of the clones (D3), the translocation was introduced via HDR using the donor DNA template, while in the second clone (G6) the translocation occurred via NHEJ. As the breakpoints were in intronic regions of the two involved genes, in both clones the transcribed and spliced RNA resulted in the typical SERPINE1-FOSB chimeric RNA. Other groups have also shown that CRISPR/Cas9 can be used to introduce chromosomal translocations in other cells, notably hMSCs via both NHEJ, but also via HDR using donor DNA templates and additional exposure to low doses of DNA-PKC inhibitor (NU7441) to block NHEJ (Vanoli et al., 2017).

Whole genome sequencing of both parental and targeted hiPSC lines showed no deleterious structural variations, copy number variations or mutations at the predicted off-target sites for the gRNAs. Any phenotypic changes observed were thus most likely associated with the *SERPINE1-FOSB* translocation.

We recently showed that overexpression of truncated *FOSB* in human umbilical vein ECs (HUVECs) recapitulated some features of PHE pathology (van Ijzendoorn et al., 2017). However, the drawback of overexpression is that they lack the regulatory elements for cell type-specific expression at levels found in tumor cells. Here we addressed the shortcomings of our previous model by introducing the truncated protein under the endogenous SERPINE1 regulatory elements via *SERPINE1-FOSB* fusion using

CRISPR/Cas9-induced translocation in hiPSCs, thereby recreating the fusion with endogenous regulatory elements of SERPINE1. We found that the *SERPINE1-FOSB* fusion results in upregulation of FOSB expression specifically in ECs, and not in undifferentiated hiPSCs, in line with known high SERPINE1 expression in vascular cells and its function as a direct transcriptional target of the activator protein 1 (AP-1) family of proteins that includes FOSB (Milde-Langosch, 2005; Walther et al., 2014). Thus, we here show that self-regulation of its own promoter, and thereby of the expression of the fusion product that is considered the driver alteration in PHE, only occurs in endothelial cells and not in undifferentiated hiPSCs. These results indicate lineage restricted expression of the fusion and confirm that PHE should be considered a vascular tumor.

Vasculogenesis assays *in vivo* in mice in which hiPSC-ECs$^{SERPINE1\text{-}FOSB\ (D3)}$ or hiPSC-ECs^{WT} were co-injected with bone marrow stromal cells (BMSCs) supported our *in vitro* findings and showed most strikingly the infiltrative growth pattern reminiscent of human PHE (Hornick and Fletcher, 2011). Vessels from hiPSC-ECs$^{SERPINE1\text{-}FOSB}$ (D3) were haphazardly arranged compared to hiPSC-ECsWT and contained higher numbers of fibrin thrombi, in two of three hiPSC-ECs$^{SERPINE1\text{-}FOSB}$ (D3). These results are in line with the *in vitro* barrier function analysis and suggest that the endothelium is aberrant inducing thrombi formation. However, some aspects of PHE were not recapitulated *in vivo.* The tumor cells typically do not form vessels in PHE but instead are spindle-shaped and co-express endothelial markers (CD31 and ERG) and keratin AE1AE3, features that are absent in our *in vivo* model. It might be that the 16 weeks time frame is not enough to develop these features in vivo. Invasion of hiPSC-ECs$^{SERPINE1\text{-}FOSB\ (D3)}$ into surrounding mouse soft tissue was observed at 16-weeks, but not at the 4-week time-point, which may suggest that the development of the phenotype takes time.

Transcriptome analysis of hiPSC-ECs with the fusion revealed differentially expressed genes associated with several pathways that are known to be related to cancer, such as TGF-beta signaling, adhesion, metabolism, inflammatory response, angiogenesis and endothelial cell migration. These are all linked to the phenotypes we observed in vitro and in vivo in our model, and recapitulate some aspects of PHE. Moreover, these pathways that we here identify to be regulated by the SERPINE1-FOSB fusion provide rationale to develop targeted treatment strategies for inoperable multifocal PHE patients. In line with our previous report of a patient with a complete clinical remission following the multi-tyrosine kinase inhibitor telatinib, we confirm upregulated MAPK signaling and overexpression of PDGFRA and -B induced by the fusion in the current model. Moreover, we identify PI3K-Akt signaling which can be targeted using mTOR inhibitors. Indeed, anecdotal responses to mTOR inhibition in patients with PHE have been reported (Gabor et al., 2018; Joseph et al., 2015; Ozeki et al., 2017).

In summary, we showed that hiPSCs and hiPSC-ECs can be used to model fusion-

driven tumors using CRISPR/Cas9 and a donor DNA template to introduce the translocation. The differentiated hiPSC-ECs carrying the pathognomonic translocation gave insights into the tumorigenesis of PHE, and elucidated the pathways regulated by the fusion product, that may provide rationale to develop targeted treatment strategies for inoperable multifocal PHE. Overall, this approach facilitated the elucidation of the role of specific fusion genes in the development of specific rare cancer subtypes for which cell lines are presently lacking.

METHODS

hiPSC lines and culture

The SeV reprogrammed hiPSC line LUMC0054iCTRL was used (additional information available in public databases: http://hpscreg.eu/cell-line/LUMCi001-A and http://hpscreg.eu/cell-line/LUMCi001-A-1) (Halaidych et al., 2018a). hiPSCs were cultured on recombinant vitronectin (VN)-coated plates in TeSR-E8 all from STEMCELL Technologies (SCT), according to the manufacturer's instructions. For targeting experiments, hiPSCs were adapted to single cell passaging on mouse embryonic fibroblasts (MEFs) in Dulbecco's modified Eagle's medium/Ham's F-12 medium (DMEM/F12) supplemented with 20% knockout serum replacement (Invitrogen), 1 mM L-glutamine, 0.1 mM nonessential amino acids, 0.1 mM 2-mercaptoethanol, and 8 ng/ml recombinant human basic fibroblast growth factor (bFGF; Milteny). Single cell adapted hiPSC were passaged using 1X TrypLE Select with additional supplementation with 1X RevitaCell (Invitrogen).

Construction of dual-guide Cas9-encoding plasmids and repair template

A dual sgRNA and Cas9-expressing plasmid was generated by introducing a second gRNA scaffold in the SpCas9-2A-Puro V2.0 (Addgene, Feng Zang) plasmid using Gibson ligation as described (Vidigal and Ventura, 2015). The final plasmid contains FOSB sgRNA TCCACTACACCGTGACGCAG and SERPINE1 sgRNA TGAACACTAGGGCAAGGTGC. The repair template was generated by blunt ligation of *FOSB* and *SERPINE1* homology arms (around 1kb each) into a P15 backbone containing a Neomycin resistance cassette surrounded by two flippase recognition target (FRT) sequences (kindly provided by Dr. Konstantinos Anastassiadis, Technical University Dresden). The CAGGs-Flpo-IRES-puro vector which expresses codon-optimized Flp recombinase was used for transient transfection to recombine FRT sites (Kranz et al., 2010) (kind gift of Dr Konstantinos Anastassiadis). The U6 vector used for the Gibson ligation was a kind gift from Dr Andrea Ventura (Addgene plasmid # 69312).

Transfection

hiPSCs were transfected at 60-70% confluence the day after seeding in a 60 mm dish.

Transfection was carried out using Lipofectamine® 2000 (Invitrogen). First, 20 µl Lipofectamine® 2000 was diluted in 300 µl Opti-MEM® Medium and incubated at RT for 5 min. In parallel, 8 µg of both the repair template and double guide RNA/Cas9 was diluted in 300 µl Opti-MEM® Medium. Diluted plasmid DNA was added to diluted Lipofectamine® 2000 in a 1:1 ratio and incubated another 5 min at RT before the DNA-lipid complex was added to the cells in a drop-wise manner. Cells were allowed to grow in the incubator for ~18 hours before the medium was changed. Antibiotic selection with 50 µg/ml G-418 was performed 24 hours post transfection and was continued for 7 days to select for targeted cells. Once recovered, cells were passaged into 6-well plates and transfected the next day with 4 µg Flp recombinase expression vector to excise the neomycin cassette (using Lipofectamine® 2000, according to the manufacturer's protocol). At 24h post transfection the medium was supplemented with 0.5 µg/ml Puromycin for 48h to enrich for transfected cells. At 80% confluence, the cells were passaged for clonal expansion on 96-well plates using limited dilution.

Fluorescence In Situ Hybridization

Three-color Fluorescence In Situ Hybridization (FISH) was performed using BAC clones (BACPAC Resource Center). Proximal to *SERPINE1* BAC clone RP11-395B7 was selected. Proximal and distal to *FOSB* respectively BAC clone RP11-84C16 and RP11-902P17 were selected. BAC DNA was extracted using the High Pure plasmid isolation kit (Roche). The RP11-395B7, RP11-84C16 and RP11-902P17 were respectively labeled with Cy5-dUTP, Fluorescein-12-dCTP and Cy3-dUTP using a nick translation labeling reaction. FISH was performed as previously described by our group (van Ijzendoorn et al., 2015). Representative images were taken using an epifluorescence microscope (Leica).

Identification of targeted hiPSC clones by PCR

PCR screening was performed to determine the presence of both the 5' homology arm of *SERPINE1* (primers SF and FR), the 3' homology arm of *FOSB* (primer F2 and R2), the wild-type *SERPINE1* (primer SF and SR) and wild-type FOSB (primer FF and FR) in clonal lines (Supplementary table 1). Colonies were picked in maximum 2 µl hESC-food and added to 20 µl QuickExtract Solution (Epicentre) in 0.5 mL tubes. The tubes were vortexed for 15s and DNA was extracted by heating the samples to 65 °C for 15 minutes, 68 °C for 15 minutes and 98 °C for 10 minutes in a thermocycler. 2-Step PCR was performed with Terra PCR Direct Polymerase (TaKaRa) according to the manufacturer's protocol. Sanger sequencing was performed (BaseClear) to confirm the *SERPINE1-FOSB* fusion and to screen the *SERPINE1* and *FOSB* wild-type allele for on-target mutations due to NHEJ.

COBRA-FISH

COmbined Binary RAtio Fluorescence in Situ Hybridization (COBRA-FISH) was performed on metaphase cells as previously described in detail(Szuhai and Tanke, 2006).

Differentiation and characterization of hiPSCs to ECs

hiPSCs were differentiated to hiPSC-ECs and characterized as previously described (Halaidych et al., 2018a; Orlova et al., 2014b; 2014a).

Real-Time qPCR

RNA isolation was performed with the Direct-zol RNA isolation kit (Zymo-research) according to the manufacturer's protocol. cDNA was synthesized using M-MLV with oligo dT primers (Promega) according to the manufacturer's protocol. Real-Time qPCR was performed with Sybr Green (Bio-Rad) on a CFX384 thermocycler (Bio-Rad). All real time PCR experiments were performed in triplicate. Primers are listed in supplementary table 2.

Western blotting

Western blotting was performed as previously described (van Ijzendoorn et al., 2017) using FOSB monoclonal rabbit antibody (#2251; Cell Signaling) and USP7 monoclonal rabbit antibody (A300-033A; Bethyl).

Assessment of hiPSC-EC proliferation

To quantify proliferation, cells were cultured in a 96-well plate for 24 hours. Presto Blue (ThermoFisher) was subsequently added to the medium and cells were incubated at 37 °C for 30 minutes before determining the Relative Fluorescence Units (RFU) using a plate reader (Perkin Elmer).

Matrigel tube formation assay

Tube formation assays were performed in 96-well plates coated with 50 µl Matrigel (Corning). hiPSC-ECs were seeded at a density of 15,000 cells per well in 150 µl EC-SFM supplemented with 1% BSA and 50 ng/µl VEGF. Tube formation was analyzed with ImageJ (NHI, v1.51s). Tube formation was imaged with the EVOS Cell Imaging System (ThermoFisher). To quantify tube formation a custom plugin in ImageJ (NIH, v1.51s) was used. Analysis scripts are available on GitHub (github.com/davidvi) for analysis of tube formation.

Endothelial barrier function and analysis

Endothelial barrier function was determined as previously described (Halaidych et al., 2018a). Briefly, hiPSC-ECs were plated on FN-coated ECIS arrays (8W10E PET, Applied Biophysics) at a density of 50,000 cells/cm^2. Wounding of the cells grown on the

electrodes was performed by applying a 10 sec pulse of 5V at 60 kHz. Barrier function was estimated by applying a current to the electrodes at 4 kHz and measuring the R [ohm]. Barrier function was measured for over 8 hours. Quantification was performed over a period of 5 hours, when the barrier had stabilized.

Immunofluorescence and immunohistochemistry

Immunofluorescence was performed as previously described (Halaidych et al., 2018a; Orlova et al., 2014a). Briefly, hiPSC-ECs were fixed with 4% PFA and permeabilized with 0.1% Triton-X100. The following primary antibodies were used: anti-ZO1 (61-7300; ThermoFisher), VEC (53-1449-42; CellSignaling), CD31 (M082301; Dako) and cells were counterstained with A488 conjugated Phalloidin (ThermoFisher). Incubation with primary antibodies was overnight at +4 °C and secondary antibodies for 30 minutes at room temperature. Immunohistochemistry with human-specific CD31 (huCD31) and FOSB was performed as previously described (Halaidych et al., 2018b). Images were acquired using EVOS FL AUTO2 Imaging System (ThermoFisher) or with the WLL1 confocal microscope (Leica), using 40x DRY objective and 0.75 Zoom factor. Used Antibodies are listed (supplementary table 3).

Vasculogenesis *in vivo* in mice

All animal experiments were performed in accordance with legal regulations with approved protocols by the Central Commissie voor Dierproeven (CCD, Central Commission for Animal Experiments). Mice were maintained at the animal facility of Leiden University Medical Center (LUMC). Teratoma and Matrigel plug assays (figure 5a) were performed in eight-week-old male NSG mice (NOD.Cg-Prkdcscid Il2rgtm1Wjl/SzJ, Charles River).

Teratoma assay

The teratoma assay was performed on the parental hiPSC^{WT} and hiPSC$^{SERPINE\text{-}FOSB\ (D3)}$ as reported before (Salvatori et al., 2018). On the same day, three animals per cell-line were injected using the same batch of cells for each mouse.

In vivo mouse Matrigel plug assay

The Matrigel plug assay was performed as described previously (Halaidych et al., 2018a; Sacchetti et al., 2016). Plugs were removed after 4 and 16 weeks. For each time points three mice were injected with hiPSC^{WT} and three mice with hiPSC$^{SERPINE\text{-}FOSB\ (D3)}$ (figure 5a). Each mouse was subcutaneously injected in the right and left flank with a mixture of hiPSC-ECs, human bone marrow-derived stromal cells (BMSCs) (PromoCell) and Matrigel (Corning). Vessel density was estimated by quantifying the human CD31^{+} area in serial sections as described previously (Halaidych et al., 2018a).

Phosphotungstic acid-haematoxylin staining and analysis

PTAH staining was performed on 4 µm FFPE sections. Paraffin was removed with xylene and sections were rehydrated in an ethanol gradient. Sections were incubated for 15 minutes in 0.25% potassium permanganate then 5 minutes in 5% oxalic acid. Last, the sections were incubated for 24 hours in PTAH solution. To analyze thrombus formation in vessels all vessels with fibrin were counted in an area of 5.7 mm^2.

Whole genome and transcriptome sequencing and analysis

DNA was isolated for whole genome sequencing using the Wizard Genomic DNA Purification Kit (Promega) and sequenced on the BGISEQ-500 platform (BGI). Reads were aligned to the GRCh38/hg19 reference genome using the Burrow-Wheeler Aligner (v0.7.12) and further processed according to the GATK (Broad institute) best practice pipeline. Copy Number Analysis (CNA) was performed using VarScan (v2.2.4) and analyzed using DNAcopy R package (v3.6). Off-target sites for the used gRNAs were determined using an online tool (crispr.cos.uni-heidelberg.de). Data was visualized with the circlize R package (v0.4.3).

RNA for transcriptome sequencing was isolated using Direct-zol RNA miniprep kit (Zymo Research). After library preparation, sequencing was performed on the BGISEQ-500 platform (BGI). Raw data was processed using the LUMC BIOPET Gentrap pipeline (https://github.com/biopet/biopet), which comprises FASTQ preprocessing, alignment and read quantification. Sickle (v1.2) was used to trim low-quality read ends15. Cutadapt (v1.1) was used for adapter clipping16, reads were aligned to the human reference genome GRCh38 using GSNAP (gmap-2014-12-23) (Wu and Nacu, 2010; Wu and Watanabe, 2005) and gene read quantification with htseq-count (v0.6.1p1) against the Ensembl v94. Gene length and GC content bias were normalized using the R package cqn (v1.28.1) (Hansen et al., 2012). Genes were excluded if the number of reads was below 5 reads in ≥90% of the samples. The final dataset comprised gene expression levels of 6 samples and 16,510 genes. Differentially expressed genes were identified using generalized linear models as implemented in (Robinson et al., 2009). P-values were adjusted using the Benjamini-Hochberg procedure and PFDR ≤ 0.05 was considered significant. Normalized RPKM values were log2 transformed and standardized across each gene using z-scores and heatmap was produced with the R package ggplot2 (v2.2.1). KEGG pathway enrichment analysis was carried out using Enrichr (Chen et al., 2013; Kuleshov et al., 2016) computational tool and $q < 0.05$ was used as the cutoff for significant pathways. Gene ontology (GO) enrichment analysis and cnetplot of selected GOs were done with R package clusterProfiler (v3.10.1) (Yu et al., 2012), $q < 0.05$ was used as the cutoff for significant GOs. Interaction networks of input genes were predicted using Interaction network analysis function of Ingenuity Pathway

Analysis (IPA) software. Then, interactions between specific genes and selected networks were generated using the Build function of IPA.

Statistical Analysis

Statistics and graphs for real-time PCR, proliferation, tube formation and barrier function were generated with GraphPad Prism (GraphPad Software). One-way ANOVA with Tukey's multiple comparison for the analysis of three or more groups or Mann-Whitney test for analysis of two groups were used. The data are reported as mean ±SD.

Data availability

Whole-genome and transcriptome sequencing data was deposited to the Sequence Read Archive under accession PRJNA448372.

Acknowledgements

We would like to thank Dr Konstantinos Anastassiadis for providing P15 backbone with a Neomycin resistance cassette surrounded by two FRT sequences and CAGGs-Flpo-IRES-puro vector, Dr Andrea Ventura for providing the U6 vector (Addgene plasmid # 69312), Dr Milena Bellin for her valuable comments on the manuscript, AE Versnel for her help in designing the figures.

JVMGB is supported by the Netherlands Organization for Scientific Research (ZON-MW VICI 016.VICI.170.055 to J.V.M.G.B.). FvdH, CLM and VVO were supported by the European Research Council (ERCAdG 323182 STEMCARDIOVASC to C.L.M.); the European Community's Seventh Framework Programme (FP7/2007-2013 under 602423); the European Union's Horizon 2020 Framework Programme (668724).

Author contributions

DGPvI conceived the study, performed experiments, collected and interpreted data and wrote the manuscript. DCFS designed and performed the animal experiments, collected and interpreted data and wrote the manuscript. XC performed analysis of RNA sequencing data. FvdH and IdB-B performed experiments. DJ performed COBRA-FISH and three-color FISH. HM performed alignment of RNA sequencing data. KS & CLM contributed to editing of the manuscript and interpreted data. VO and JB conceived the study, interpreted data and wrote the manuscript.

REFERENCES

Billings, S.D., Folpe, A.L., Weiss, S.W., 2003. Epithelioid sarcoma-like hemangioendothelioma. The American Journal of Surgical Pathology 27, 48–57. doi:10.1097/00000478-200301000-00006

Cantelmo, A.R., Conradi, L.-C., Brajic, A., Goveia, J., Kalucka, J., Pircher, A., Chaturvedi, P., Hol, J., Thienpont, B., Teuwen, L.-A., Schoors, S., Boeckx, B., Vriens, J., Kuchnio, A., Veys, K., Cruys, B., Finotto, L., Treps, L., Stav-Noraas, T.E., Bifari, F., Stapor, P., Decimo, I., Kampen, K., De Bock, K., Haraldsen, G., Schoonjans, L., Rabelink, T., Eelen, G., Ghesquière, B., Rehman, J., Lambrechts, D., Malik, A.B., Dewerchin, M., Carmeliet, P., 2016. Inhibition of the Glycolytic Activator PFKFB3 in Endothelium Induces Tumor Vessel Normalization, Impairs Metastasis, and Improves Chemotherapy. Cancer Cell 30, 968–985. doi:10.1016/j.ccell.2016.10.006

Chen, E.Y., Tan, C.M., Kou, Y., Duan, Q., Wang, Z., Meirelles, G., Clark, N.R., Ma'ayan, A., 2013. Enrichr: interactive and collaborative HTML5 gene list enrichment analysis tool. BMC Bioinformatics 14, 128. doi:10.1186/1471-2105-14-128

Gabor, K.M., Sapi, Z., Tiszlavicz, L.G., Fige, A., Bereczki, C., Bartyik, K., 2018. Sirolimus therapy in the treatment of pseudomyogenic hemangioendothelioma. Pediatr Blood Cancer 65, e26781. doi:10.1002/pbc.26781

Halaidych, O.V., Freund, C., van den Hil, F., Salvatori, D.C.F., Riminucci, M., Mummery, C.L., Orlova, V.V., 2018a. Inflammatory Responses and Barrier Function of Endothelial Cells Derived from Human Induced Pluripotent Stem Cells. STEMCR 10, 1642–1656. doi:10.1016/j.stemcr.2018.03.012

Halaidych, O.V., Freund, C., van den Hil, F., Salvatori, D.C.F., Riminucci, M., Mummery, C.L., Orlova, V.V., 2018b. Inflammatory Responses and Barrier Function of Endothelial Cells Derived from Human Induced Pluripotent Stem Cells. STEMCR 10, 1642–1656. doi:10.1016/j.stemcr.2018.03.012

Hansen, K.D., Irizarry, R.A., Wu, Z., 2012. Removing technical variability in RNA-seq data using conditional quantile normalization. Biostatistics 13, 204–216. doi:10.1093/biostatistics/kxr054

Hornick, J.L., Fletcher, C.D.M., 2011. Pseudomyogenic hemangioendothelioma: a distinctive, often multicentric tumor with indolent behavior. The American Journal of Surgical Pathology 35, 190–201. doi:10.1097/PAS.0b013e3181ff0901

Hung, Y.P., Fletcher, C.D.M., Hornick, J.L., 2017. FOSB is a Useful Diagnostic Marker for Pseudomyogenic Hemangioendothelioma. The American Journal of Surgical Pathology 41, 596–606. doi:10.1097/PAS.0000000000000795

Ide, Y.-H., Tsukamoto, Y., Ito, T., Watanabe, T., Nakagawa, N., Haneda, T., Nagai, M., Yamanishi, K., Hirota, S., 2015. Penile pseudomyogenic hemangioendothelioma/epithelioid sarcoma-like hemangioendothelioma with a novel pattern of SERPINE1-FOSB fusion detected by RT-PCR – Report of a case. Pathology -- Research and Practice 211, 415–420. doi:10.1016/j.prp.2015.02.003

Joseph, J., Wang, W.-L., Patnana, M., Ramesh, N., Benjamin, R., Patel, S., Ravi, V., 2015. Cytotoxic and targeted therapy for treatment of pseudomyogenic hemangioendothelioma. Clinical Sarcoma Research 5, 22–6. doi:10.1186/s13569-015-0037-8

Kranz, A., Fu, J., Duerschke, K., Weidlich, S., Naumann, R., Stewart, A.F., Anastassiadis, K., 2010.

An improved Flp deleter mouse in C57Bl/6 based on Flpo recombinase. genesis 48, 512–520. doi:10.1002/dvg.20641

Kuleshov, M.V., Jones, M.R., Rouillard, A.D., Fernandez, N.F., Duan, Q., Wang, Z., Koplev, S., Jenkins, S.L., Jagodnik, K.M., Lachmann, A., McDermott, M.G., Monteiro, C.D., Gundersen, G.W., Ma'ayan, A., 2016. Enrichr: a comprehensive gene set enrichment analysis web server 2016 update. Nucleic Acids Research 44, W90–W97. doi:10.1093/nar/gkw377

Mertens, F., Antonescu, C.R., Mitelman, F., 2016. Gene fusions in soft tissue tumors: Recurrent and overlapping pathogenetic themes. Genes Chromosomes Cancer 55, 291–310. doi:10.1002/gcc.22335

Milde-Langosch, K., 2005. The Fos family of transcription factors and their role in tumourigenesis. European Journal of Cancer 41, 2449–2461. doi:10.1016/j.ejca.2005.08.008

Miller, D.W., Graulich, W., Karges, B., Stahl, S., Ernst, M., Ramaswamy, A., Sedlacek, H.H., Müller, R., Adamkiewicz, J., 1999. Elevated expression of endoglin, a component of the TGF-beta-receptor complex, correlates with proliferation of tumor endothelial cells. Int. J. Cancer 81, 568–572. doi:10.1002/(sici)1097-0215(19990517)81:4<568::aid-ijc11>3.0.co;2-x

Mitelman, F., Johansson, B., Mertens, F., 2007. The impact of translocations and gene fusions on cancer causation. Nat Rev Cancer 7, 233–245. doi:10.1038/nrc2091

Orlova, V.V., Drabsch, Y., Freund, C., Petrus-Reurer, S., van den Hil, F.E., Muenthaisong, S., Dijke, P.T., Mummery, C.L., 2014a. Functionality of endothelial cells and pericytes from human pluripotent stem cells demonstrated in cultured vascular plexus and zebrafish xenografts. Arteriosclerosis, Thrombosis, and Vascular Biology 34, 177–186. doi:10.1161/ATVBAHA.113.302598

Orlova, V.V., van den Hil, F.E., Petrus-Reurer, S., Drabsch, Y., Dijke, ten, P., Mummery, C.L., 2014b. Generation, expansion and functional analysis of endothelial cells and pericytes derived from human pluripotent stem cells. Nature Protocols 9, 1514–1531. doi:10.1038/nprot.2014.102

Ozeki, M., Nozawa, A., Kanda, K., Hori, T., Nagano, A., Shimada, A., Miyazaki, T., Fukao, T., 2017. Everolimus for Treatment of Pseudomyogenic Hemangioendothelioma. J. Pediatr. Hematol. Oncol. 39, e328–e331. doi:10.1097/MPH.0000000000000778

Robinson, M.D., McCarthy, D.J., Smyth, G.K., 2009. edgeR: a Bioconductor package for differential expression analysis of digital gene expression data. Bioinformatics 26, 139–140. doi:10.1093/bioinformatics/btp616

Sacchetti, B., Funari, A., Remoli, C., Giannicola, G., Kogler, G., Liedtke, S., Cossu, G., Serafini, M., Sampaolesi, M., Tagliafico, E., Tenedini, E., Saggio, I., Robey, P.G., Riminucci, M., Bianco, P., 2016. No Identical "Mesenchymal Stem Cells" at Different Times and Sites: Human Committed Progenitors of Distinct Origin and Differentiation Potential Are Incorporated as Adventitial Cells in Microvessels. STEMCR 6, 897–913. doi:10.1016/j.stemcr.2016.05.011

Salvatori, D.C.F., Dorssers, L.C.J., Gillis, A.J.M., Perretta, G., van Agthoven, T., Gomes Fernandes, M., Stoop, H., Prins, J.-B., Oosterhuis, J.W., Mummery, C., Looijenga, L.H.J., 2018. The

MicroRNA-371 Family as Plasma Biomarkers for Monitoring Undifferentiated and Potentially Malignant Human Pluripotent Stem Cells in Teratoma Assays. STEMCR 11, 1493–1505. doi:10.1016/j.stemcr.2018.11.002

Sánchez-Rivera, F.J., Jacks, T., 2015. Applications of the CRISPR–Cas9 system in cancer biology. Nat Rev Cancer 15, 387–393. doi:10.1038/nrc3950

Schneidawind, C., Jeong, J., Schneidawind, D., Kim, I.-S., Duque-Afonso, J., Wong, S.H.K., Iwasaki, M., Breese, E.H., Zehnder, J.L., Porteus, M., Cleary, M.L., 2018. MLL leukemia induction by t(9;11) chromosomal translocation in human hematopoietic stem cells using genome editing. Blood Adv 2, 832–845. doi:10.1182/bloodadvances.2017013748

Szuhai, K., Tanke, H.J., 2006. COBRA: combined binary ratio labeling of nucleic-acid probes for multi-color fluorescence in situ hybridization karyotyping. Nature Protocols 1, 264–275. doi:10.1038/nprot.2006.41

Takahashi, K., Tanabe, K., Ohnuki, M., Narita, M., Ichisaka, T., Tomoda, K., Yamanaka, S., 2007. Induction of pluripotent stem cells from adult human fibroblasts by defined factors. Cell 131, 861–872. doi:10.1016/j.cell.2007.11.019

Torres, R., Martin, M.C., Garcia, A., Cigudosa, J.C., Ramirez, J.C., Rodriguez-Perales, S., 2014. Engineering human tumour-associated chromosomal translocations with the RNA-guided CRISPR-Cas9 system. Nature Communications 5, 3964. doi:10.1038/ncomms4964

Torres-Ruiz, R., Martinez-Lage, M., Martin, M.C., Garcia, A., Bueno, C., Castaño, J., Ramirez, J.C., Menendez, P., Cigudosa, J.C., Rodriguez-Perales, S., 2017. Efficient Recreation of t(11;22) EWSR1-FLI1+ in Human Stem Cells Using CRISPR/Cas9. STEMCR 8, 1408–1420. doi:10.1016/j.stemcr.2017.04.014

Trombetta, D., Magnusson, L., Steyern, von, F.V., Hornick, J.L., Fletcher, C.D.M., Mertens, F., 2011. Translocation t(7;19)(q22;q13)−a recurrent chromosome aberration in pseudomyogenic hemangioendothelioma? Cancer Genet 204, 211–215. doi:10.1016/j.cancergen.2011.01.002

van Ijzendoorn, D.G.P., de Jong, D., Romagosa, C., Picci, P., Benassi, M.S., Gambarotti, M., Daugaard, S., van de Sande, M., Szuhai, K., Bovée, J.V.M.G., 2015. Fusion events lead to truncation of FOS in epithelioid hemangioma of bone. Genes Chromosomes Cancer 54, 565–574. doi:10.1002/gcc.22269

van Ijzendoorn, D.G.P., Forghany, Z., Liebelt, F., Vertegaal, A.C., Jochemsen, A.G., Bovée, J.V.M.G., Szuhai, K., Baker, D.A., 2017. Functional Analyses of a Human Vascular Tumor FOS Variant Identify a Novel Degradation Mechanism and a link to Tumorigenesis. Journal of Biological Chemistry jbc.C117.815845–21. doi:10.1074/jbc.C117.815845

van IJzendoorn, D.G.P., Sleijfer, S., Gelderblom, H., Eskens, F.A.L.M., van Leenders, G.J., Szuhai, K., Bovée, J.V.M.G., 2018. Telatinib is an effective targeted therapy for pseudomyogenic hemangioendothelioma. Clinical Cancer Research clincanres.3512.2017–22. doi:10.1158/1078-0432.CCR-17-3512

Vanoli, F., Tomishima, M., Feng, W., Lamribet, K., Babin, L., Brunet, E., Jasin, M., 2017. CRISPR-

Cas9–guided oncogenic chromosomal translocations with conditional fusion protein expression in human mesenchymal cells. Proceedings of the National Academy of Sciences 114, 3696–3701. doi:10.1073/pnas.1700622114

Verbeke, S.L.J., Bertoni, F., Bacchini, P., Oosting, J., Sciot, R., Krenács, T., Bovée, J.V.M.G., 2013. Active TGF-β signaling and decreased expression of PTEN separates angiosarcoma of bone from its soft tissue counterpart. Mod. Pathol. 26, 1211–1221. doi:10.1038/modpathol.2013.56

Vidigal, J.A., Ventura, A., 2015. Rapid and efficient one-step generation of paired gRNA CRISPR-Cas9 libraries. Nature Communications 6, 8083–7. doi:10.1038/ncomms9083

Walther, C., Tayebwa, J., Lilljebjörn, H., Magnusson, L., Nilsson, J., Steyern, von, F.V., Øra, I., Domanski, H.A., Fioretos, T., Nord, K.H., Fletcher, C.D., Mertens, F., 2014. A novel SERPINE1-FOSBfusion gene results in transcriptional up-regulation of FOSBin pseudomyogenic haemangioendothelioma. J. Pathol. 232, 534–540. doi:10.1002/path.4322

Wu, T.D., Nacu, S., 2010. Fast and SNP-tolerant detection of complex variants and splicing in short reads. Bioinformatics 26, 873–881. doi:10.1093/bioinformatics/btq057

Wu, T.D., Watanabe, C.K., 2005. GMAP: a genomic mapping and alignment program for mRNA and EST sequences. Bioinformatics 21, 1859–1875. doi:10.1093/bioinformatics/bti310

Yu, G., Wang, L.-G., Han, Y., He, Q.-Y., 2012. clusterProfiler: an R package for comparing biological themes among gene clusters. OMICS 16, 284–287. doi:10.1089/omi.2011.0118

SUPPLEMENTARY INFORMATION

Supplementary Figures S1-S5

Supplementary Tables 1-3

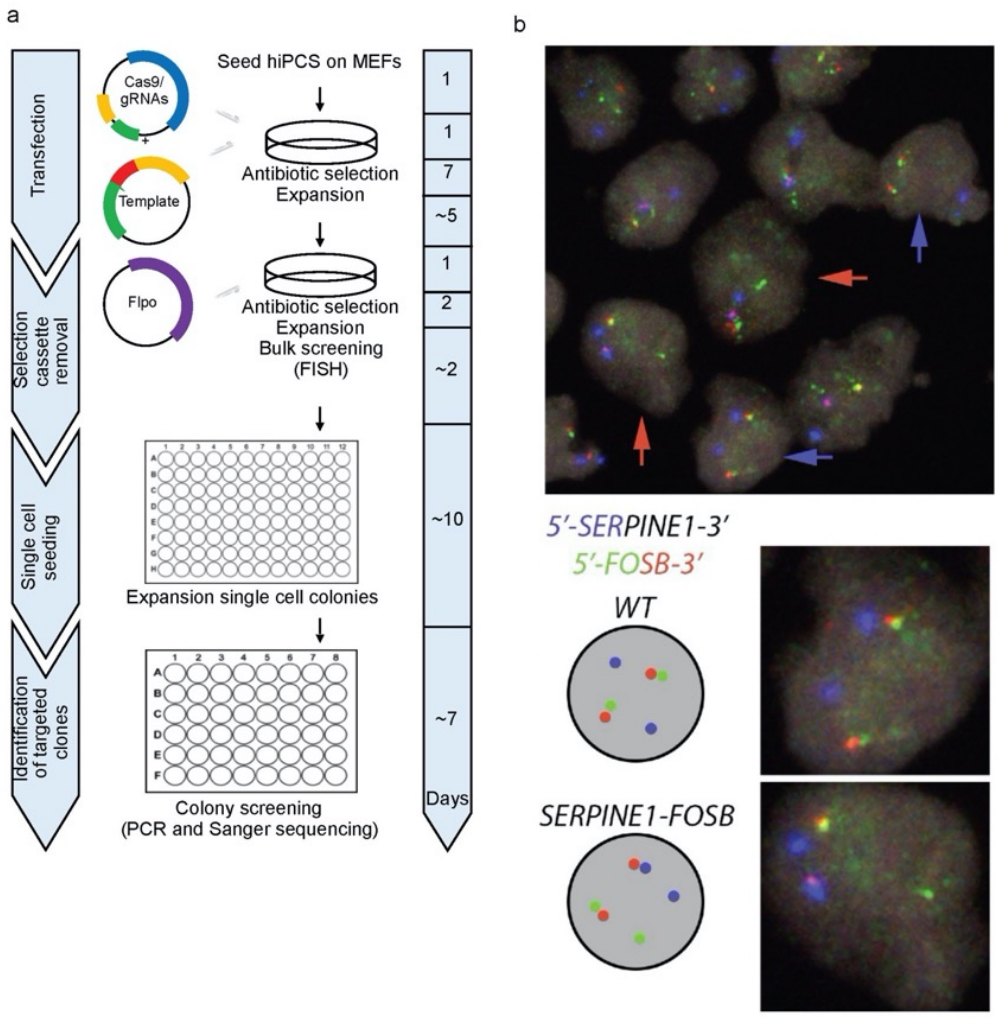

Supplementary figure S1. Generation and characterization of hiPSCs with a *SERPINE-FOSB* fusion. (a) Schematic overview of the targeting and screening experimental workflow. (b) Three color FISH (Blue at 5' side of *SERPINE1*; green at 5' side of *FOSB* and red at 3' side of *FOSB*) for the detection of *SERPINE1-FOSB* fusion on hiPSC "bulk" culture prior to single-cell deposition. Red arrows indicate cells with the fusion, and blue arrows show wild-type cells. The right image shows a schematic and representative overview of targeted and wild-type cells, as detected with three color FISH.

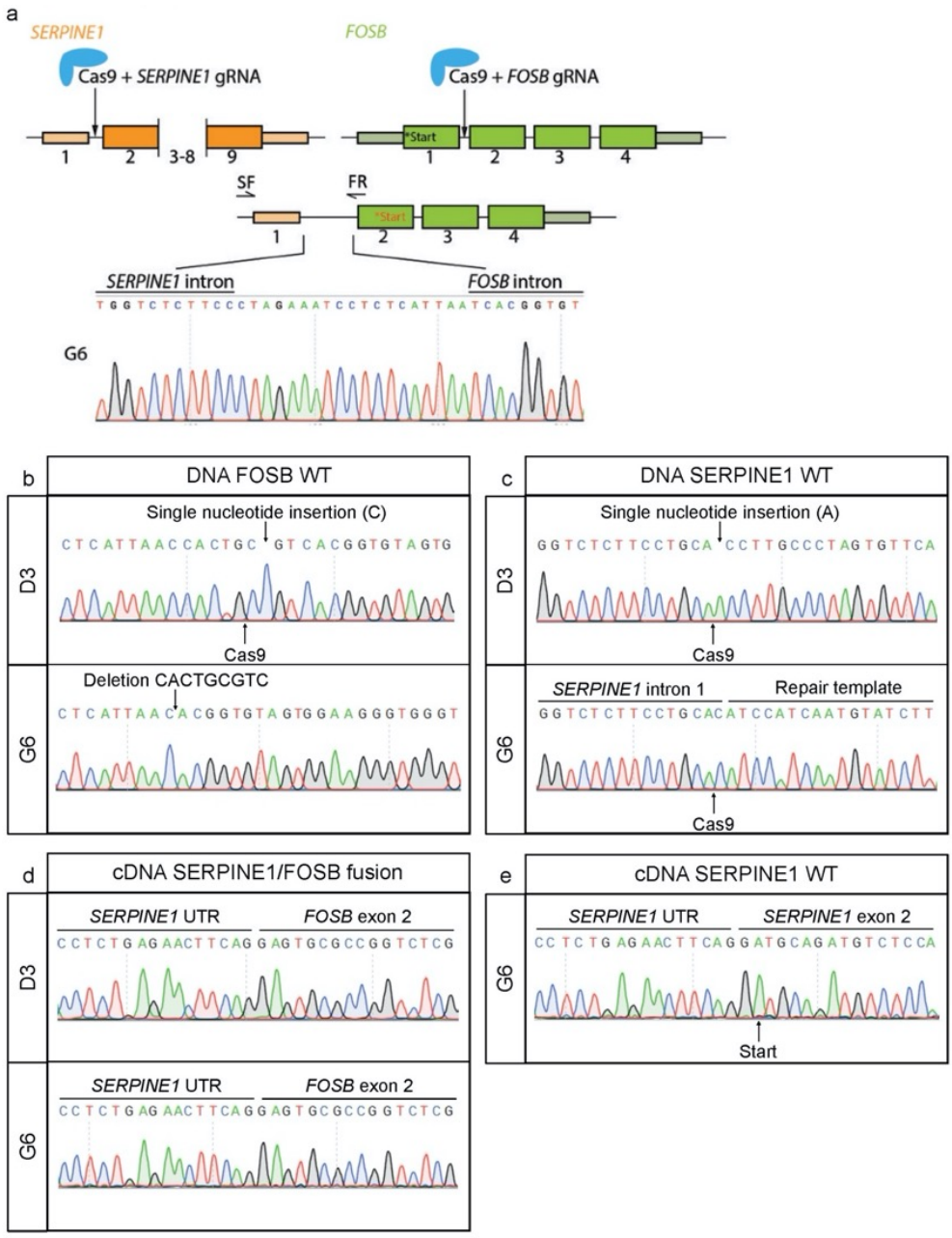

Supplementary figure S2. Sanger sequencing of hiPSCs with a *SERPINE-FOSB* fusion. (a) Upper panel: schematic overview of NHEJ-mediated repair resulting in generation of clone G6. Bottom panel: Sanger sequencing of PCR products from G6 clone validating NHEJ recombination of SERPINE1 and FOSB with a random piece of DNA inserted in the intron between the fusion. (b,c) Sanger sequencing of the non-targeted wild-type FOSB intron 1 and wild-type SERPINE1 intron 1 in hiPSC clones D3 and G6. (d) Sanger sequencing of cDNA from clones D3 and G6 showing normal splicing of fusion SERPINE1-FOSB mRNA using forward primer on the SERPINE1 UTR and a reverse primer on FOSB exon 3. (e) Sanger sequencing of the non-targeted wild-type

SERPINE1 cDNA with primers on the SERPINE1 UTR and exon 2 showing that the insertion of the selection cassette fragment had no effect on splicing of SERPINE1 mRNA in colony G6.

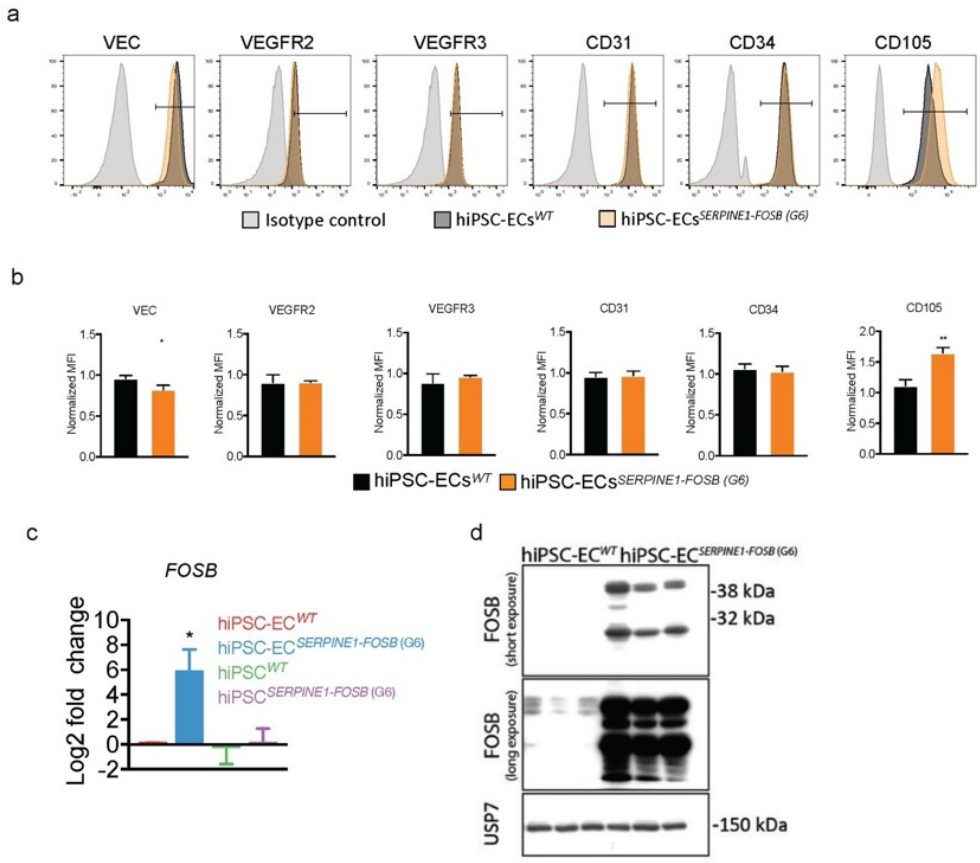

Supplementary figure S3. Characterization of hiPSC-ECs with *SERPINE1-FOSB* fusion. (a) FACS analysis of EC markers expression on isolated hiPSC-ECs^{WT} (black filled histogram) and hiPSC-ECs$^{SERPINE-FOSB\ (G6)}$ (orange filled histogram) at passage 2 (P2) and relevant isotype control (gray filled histogram). **(b)** Quantification of relative surface expression levels (MFI) of VEC, VEGFR2, VEGFR3, CD31, CD34 and CD105. Experiments were performed in triplicate with three independent batches of hiPSC-ECs. Error bars are SD. **(c)** Real-time qPCR analysis of *FOSB* expression in hiPSCs^{WT}, hiPSCs$^{SERPINE1-FOSB\ (G6)}$, hiPSC-ECs^{WT} and hiPSC-ECs$^{SERPINE1-FOSB\ (G6)}$. Experiments were performed with three independent batches of hiPSC-ECs. Expression is determined relative to hiPSC-ECs^{WT}, shown as log2 fold change. Error bars are SD. * p<0.005. (d) Western blot analysis of FOSB expression in hiPSC-ECs^{WT} and hiPSC-ECs$^{SERPINE1-FOSB}$ (G6). USP7 was used as a housekeeping control.

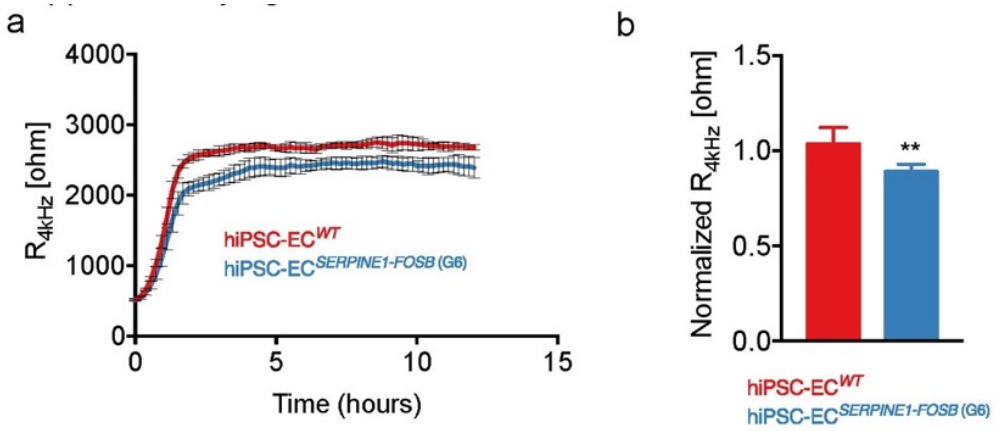

Supplementary figure S4. Assessment of barrier function of hiPSC-ECs with *SERPINE1-FOSB* fusion.

(a) Representative absolute resistance of the hiPSC-EC monolayer in complete EC growth medium. Errors bars are shown as ±SD. **(b)** Normalized resistance [4 kHz] of the hiPSC-EC monolayer in complete EC growth medium. Error bars are shown as ±SD of six independent biological experiments. *** p<0.001. Experiments were performed in triplicate using three independent batches of hiPSC-ECs.

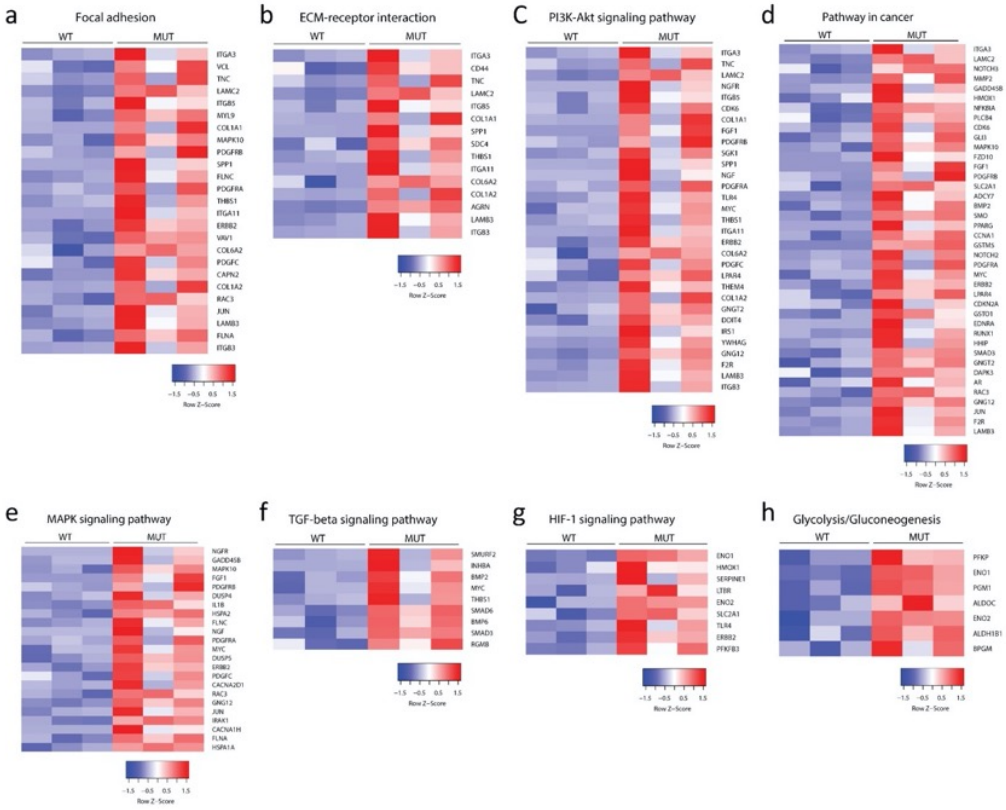

Supplementary figure S5. KEGG pathways identified in hiPSC-ECs$^{SERPINE1\text{-}FOSB\ (D3)}$ upregulated DEGs.

(a-h) Heatmaps of genes from eight representative KEGG pathways enriched in hiPSC-ECs$^{SERPINE1\text{-}FOSB(D3)}$ upregulated DEGs.

Supplementary table 1: PCR primers used to screen targeted clones.

Name	Sequence
SERPINE1 (SF)	ACACAGGCAGAGGGCAGAAAGGTCAA
SERPINE1 (SR)	CCTGCGCCACCTGCTGAAACAC
FOSB (FF)	GCCTTCAGAGCAGTTCCAGGAGTCCATTTA
FOSB (FR)	ACCGACACACACACACCCAACACACATAA
F2	TGGGCTGCAAAGGCAGAGAGTGGTAAT
R2	AAGCGATCCTCCCACTAAAGCCTCCATAGT

Supplementary table 2: qPCR primers.

Name	Sequence
HPRT_f	TGACACTGGCAAAACAATGCA
HPRT_r	GGTCCTTTTCACCAGCAAGCT
FOSB_f	AGCAGCAGCTAAATGCAGGA
FOSB_r	CCAACTGATCTGTCTCCGCC

Supplementary table 3: Antibodies and their dilutions.

Antibody	Cat#	Manufacturer	Clone	Dilutions
VE-cadherin-A488	53-1449-42	eBiosciences	16B1	1:100
KDR-PE	FAB357P	R&D systems	89106	1:50
VEGFR3-PE	FAB3492P	R&D systems	54733	1:50
CD31-APC	17-0319-42	eBiosciences	WM59	1:200
CD34- PerCP-Cy5.5	347222	BD Pharmingen	8G12	1:100
CD105-VioBlue	130-099-666	Miltenyi Biotec	43A4E1	1:50
Phalloidin-A488	A12379	ThermoFisher	N/A	1:20

VE-Cadherin	2158S	Cell Signaling	Polyclonal	1:200
ZO-1	61-7300	ThermoFisher	Polyclonal	1:200?
CD31	M0823	Dako	JC70A	1:200 IF 1:30 IHC
FOSB	2251S	Cell Signaling	5G4	1:200 IF 1:30000 WB
USP7	A300-033A	Bethyl Laboratories	Polyclonal	1:10000

Appendix Chapter 6:

Follow up bioinformatics analysis of hiPSC-endothelial cells expressing the *SERPINE1-FOSB* translocation

Xu Cao[1], Judith V.M.G. Bovée[2], Christine L. Mummery[1], Valeria V. Orlova[1,*]
[1]Department of Anatomy and Embryology, Leiden University Medical Center, Leiden, The Netherlands
[2]Department of Pathology, Leiden University Medical Center, Leiden, The Netherlands
[*]Correspondence: v.orlova@lumc.nl

Abstract
Establishing an *in vitro* model of Pseudomyogenic hemangioendothelioma (PHE) using human induced pluripotent stem cells (hiPSCs) would provide a powerful tool for the study of pathology and rationale for treatment strategies. In **Chapter 6**, we generated a PHE hiPSC line by introducing the chromosomal translocation into wild type (WT) hiPSCs using CRISPR/Cas9 and established a disease model of PHE with hiPSC-endothelial cells (hiPSC-ECs). RNA sequencing (RNAseq) analysis of hiPSC-ECs described in **Chapter 6** gave an initial in-depth view on the disease mechanism at the gene expression and signaling pathway levels. In this chapter (appendix chapter 6), I describe and extended RNAseq analysis for this disease model. This bioinformatic analysis provided extra information on the dysregulated transcriptional networks in mutated ECs that are relevant for the disease pathologies in PHE. Most importantly, candidate drug targets are predicted here based on Ingenuity pathway analysis (IPA). These offer new potential treatment opportunities for PHE.

Introduction
In Chapter 6, we established an *in vitro* model of Pseudomyogenic hemangioendothelioma (PHE) using human induced pluripotent stem cell-derived ECs (hiPSC-ECs) carrying the *SERPINE1-FOSB* translocation. hiPSC-ECs$^{SERPINE1\text{-}FOSB}$ showed several disease phenotypes *in vitro* and in mice after transplantation, which resembling certain aspects of the PHE phenotype observed in patients (Hornick and Fletcher, 2011). Whole transcriptome sequencing and bioinformatic analysis performed in **Chapter 6** for the hiPSC model provided a powerful approach to revealing dysregulated transcription networks as a result of the translocation and indications of underlying disease

mechanisms of PHE. The transcriptome of ECs derived from wild type (WT) and mutated hiPSCs were compared and dysregulated genes in hiPSC-ECs$^{SERPINE1\text{-}FOSB}$ were identified. Gene Ontology (GO) and KEGG pathway enrichment analysis were the performed to identify signaling pathways and cellular activities linked to these differentially expressed genes (DEGs). Ingenuity pathway analysis (IPA) was next performed to investigate the gene regulation networks between DEGs and thus reveal new pathways underlying disease pathologies. These RNAseq analyses provided the rationale for new therapeutic strategies that could be used for PHE. However, only the most critical RNAseq analysis results were included in **Chapter 6** due to the restriction of the length of the article.

Here, we present additional RNAseq analysis carried out in this hiPSC model of PHE. Although beyond the scope of the manuscript in chapter 6, the data are valuable and informative in terms of the understanding the pathology and development of treatment strategies for PHE. WT and mutated hiPSC-ECs together with hiPSCs were included in the bioinformatic analysis. Additional gene-gene interaction- and regulatory networks of DEGs between WT and mutated hiPSC-ECs were identified; Two candidate drugs that target on dysregulated genes of hiPSC-ECs$^{SERPINE1\text{-}FOSB}$ were predicted using a powerful bioinformatic tool IPA. This extra bioinformatic analysis not only complemented the RNAseq analysis in **Chapter 6**, but also give new insights into the disease mechanism and drug development for PHE.

Results

Transcriptome analysis of hiPSCs and hiPSC-ECs with and without *SERPINE1-FOSB* translocation.

To obtain an overview of cell identities and transcriptome profiles, principle component analysis was performed for WT hiPSCs, hiPSC-EC^{WT} and hiPSC-ECs$^{SERPINE1\text{-}FOSB}$, with three replicates in each group (Figure 1a). Samples from the same group clustered together. hiPSC samples clustered separately from EC samples by PC1, while hiPSC-EC^{WT} and hiPSC-EC$^{SERPINE1\text{-}FOSB}$ are separated principally by PC2 (Figure 1a). hiPSC-ECs$^{SERPINE1\text{-}FOSB}$ samples showed the highest variation within the group compared to other groups. 1222 DEGs identified between hiPSC-EC^{WT} and hiPSC-EC$^{SERPINE1\text{-}FOSB}$ (see **Chapter 6**) were divided into 4 clusters based on their expression pattern in different groups (Figure 1b). Cluster 1 genes are highest in hiPSCs and lowest in hiPSC-EC^{WT}. Cluster 2 genes are highest in hiPSCs but also present in hiPSC-EC$^{SERPINE1\text{-}FOSB}$. Cluster 3 and 4 genes are mainly expressed by ECs. Cluster 3 was higher in hiPSC-EC^{WT}, while cluster 4 was higher in hiPSC-EC$^{SERPINE1\text{-}FOSB}$.

To characterize genes in each cluster, GO enrichment analysis was performed with the cluster Profiler R package (Figure 1c). Mucosal immune response was enriched in cluster 1. A large number of GOs including extracellular matrix organization, cell growth, regeneration, asymmetric cell division were identified in cluster 2. Cluster 3 genes were

mainly related to immune responses. Meanwhile, genes in cluster 4 were associated with processes like angiogenesis, cell migration, endothelial cell proliferation, response to transforming growth factor beta, regulation of ERK1 and ERK2 cascade.

Gene-gene interaction analysis for dysregulated genes in hiPSC-EC$^{SERPINE1\text{-}FOSB}$

To investigate the interaction between *SERPINE1-FOSB* translocation and dysregulated genes/signaling pathways, IPA was applied for DEGs between hiPSC-EC^{WT} and hiPSC-EC$^{SERPINE1\text{-}FOSB}$. First, upstream and downstream genes which have direct connections with *FOSB* and *SERPINE1* were identified. Interactions among these identified genes were thus revealed. All of these genes and interactions were mapped based on their cellular positions as shown in Figure 2a. *FOSB* regulates *SERPINE1* expression directly. Both *FOSB* and *SERPINE1* show self-regulatory effects. *FOSB* is regulated by several extracellular growth factors, like TGFB3, IGF1, HGF, GDNF, FGF2. Many upstream regulators of *FOSB* and *SERPINE1* were expressed at higher levels in hiPSC-EC$^{SERPINE1\text{-}FOSB}$ than hiPSC-EC^{WT} (Figure 2a, labeled in green).

Next, regulatory effects among upregulated genes of hiPSC-EC$^{SERPINE1\text{-}FOSB}$ were identified using IPA software, which allowed us to identify upstream regulators as well as downstream cellular function and activities (similar to GO enrichment) linked to these genes. ADA and LOX were found to promote the expression of most upregulated genes in hiPSC-EC$^{SERPINE1\text{-}FOSB}$ (Figure 2b). These upregulated genes are involved in many cellular processes, including angiogenesis, vascularization, invasion of tumor cells, cell proliferation of tumor cells, mitogenesis et al. (Figure 2b).

Potential drugs predicted by IPA that target on dysregulated genes in hiPSC-EC$^{SERPINE1\text{-}FOSB}$

Using the Drug prediction function incorporated in IPA software, two candidate drugs were identified which could inhibit the expression of upregulated genes in hiPSC-EC$^{SERPINE1\text{-}FOSB}$. Both LY294002 and PD98059 were identifid as inhibitors of a large number of dysregulated genes caused by the *SERPINE1-FOSB* translocation. LY294002 can inhibit *FOSB* expression but promote *SERPINE1* expression, while PD98059 inhibits expression of both *FOSB* and *SERPINE1*.

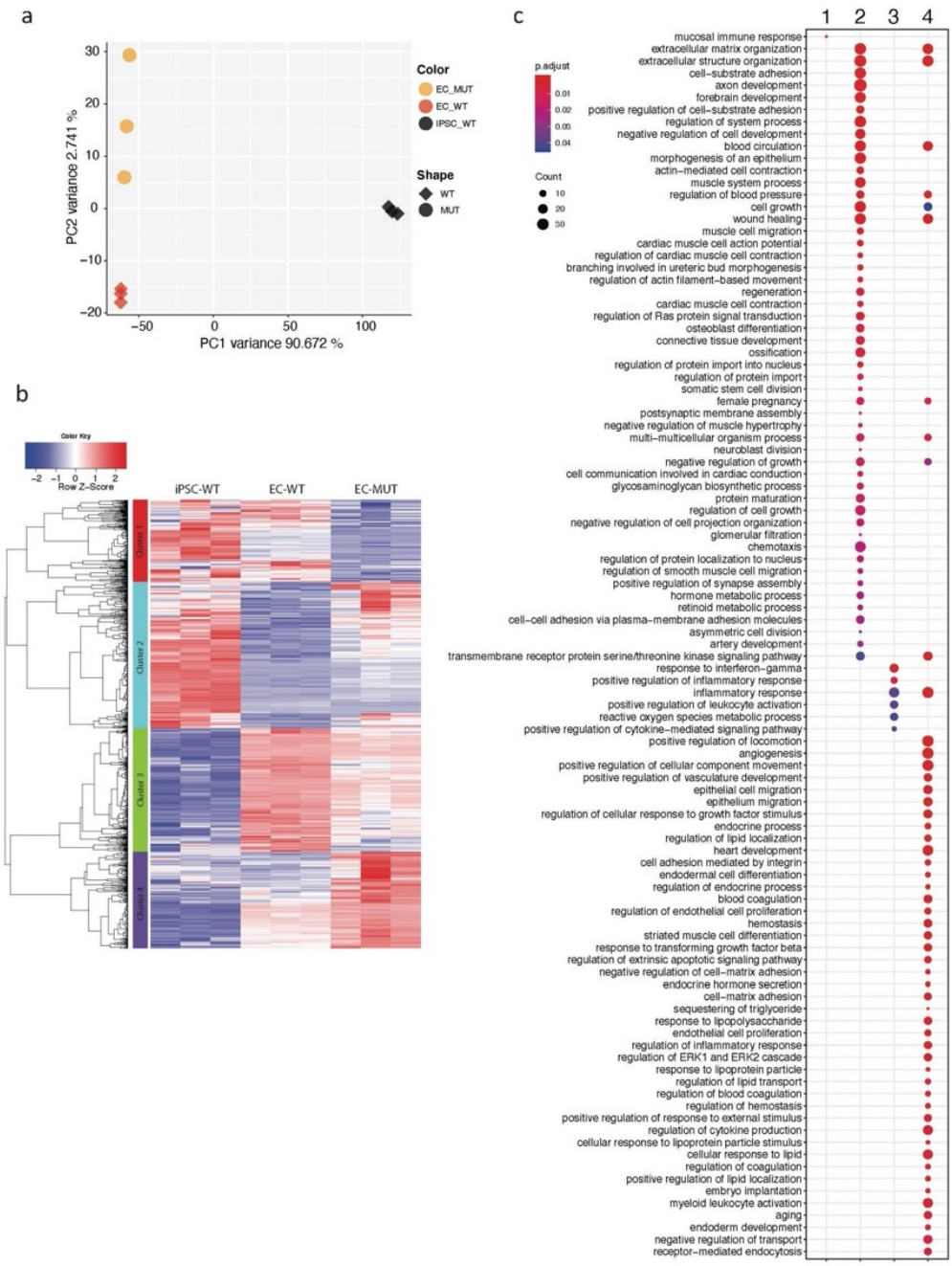

Figure 1. Transcriptome analysis of hiPSCs and hiPSC-ECs with and without *SERPINE1-FOSB* translocation. (a) Principle component analysis (PCA) of hiPSCs and hiPSC-ECs with (EC_MUT) and without (EC_WT) *SERPINE1-FOSB* translocation. (b) Hierarchical clustering analysis for 1222 differentially expressed genes (DEGs) between EC_MUT and EC_WT. All genes were divided into 4 clusters by setting Cutree to 4. (c) Gene Ontology (GO) enrichment for each cluster of genes using clusterProfiler R package.

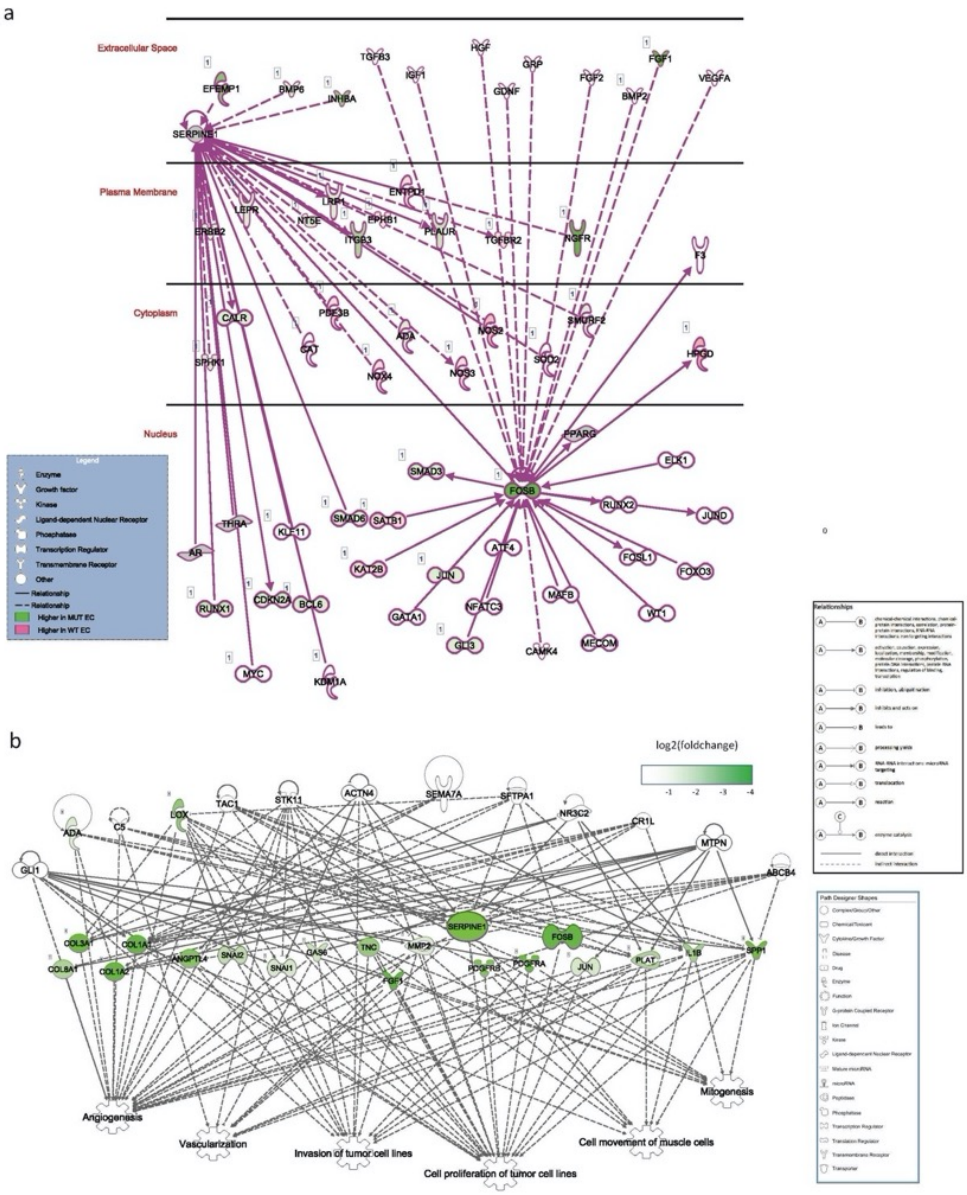

Figure 2. Gene-gene interaction analysis for DEGs between hiPSC-ECs with and without *SERPINE1-FOSB* translocation. (a) Gene-gene interactions of *SERPINE1*- and *FOSB*-regulated genes predicated by Integrity pathway analysis (IPA). Cellular positions of these genes were illustrated. (b) Regulator effects predicated by Integrity pathway analysis (IPA) for genes shown in Figure 5d. Upstream regulators and downstream functions/diseases are shown as a network. Color indicates the log2(fold change) of gene expression in MUT compared to WT.

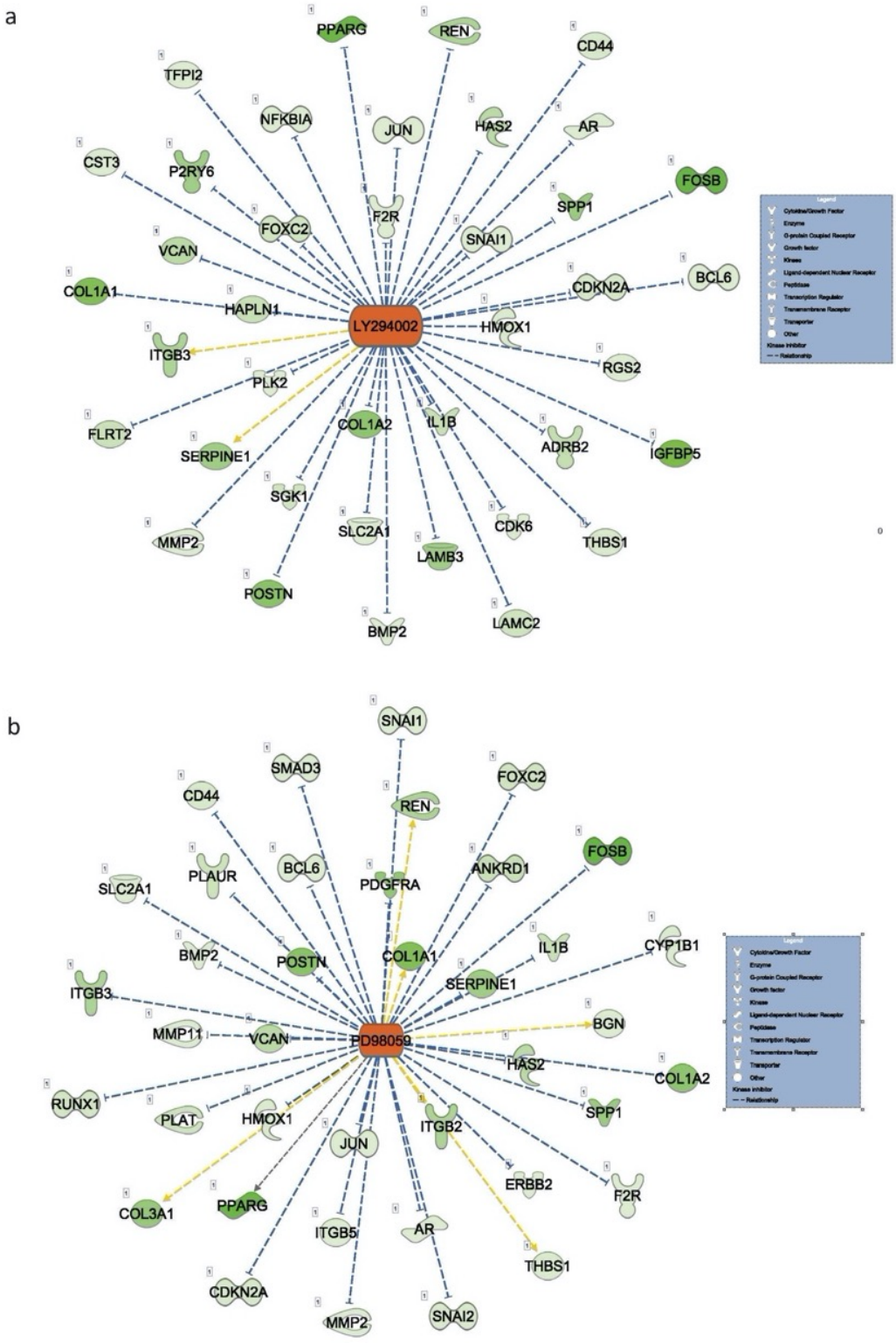

Figure 3. Two drugs called LY294002 (a) and PD98059 (b) predicted by IPA which could inhibit

dysregulated genes that higher in MUT ECs compared to WT ECs.

Discussion

In this chapter appendix, we included extra bioinformatic analysis for the transcriptome profiles of hiPSCs and hiPSC-ECs with and without *SERPINE1-FOSB* translocation, which reveal important new information but could not be included in **Chapter 6** for space reasons. We found that hiPSC-ECs carrying the *SERPINE1-FOSB* translocation preserved a clear EC identity that was distinct from undifferentiated hiPSCs. Around half of DEGs between hiPSC-EC^{WT} and hiPSC-EC$^{SERPINE1\text{-}FOSB}$ were hiPSCs specific genes. Interestingly, a large number of hiPSCs specific genes (cluster 2) were upregulated only in hiPSC-EC$^{SERPINE1\text{-}FOSB}$ but not in hiPSC-EC^{WT}. These genes are involved in cell proliferation and migration, which correlated with the PHE tumor phenotypes in patients and the hiPSC model established in **Chapter 6**. Genes related to EC proliferation, response to transforming growth factor beta and regulation of inflammatory response were upregulated in hiPSC-EC$^{SERPINE1\text{-}FOSB}$, which also correlated with the abnormal phenotypes observed with hiPSC-EC$^{SERPINE1\text{-}FOSB}$ *in vitro,* like aberrant cell barrier function and formation of haphazardly arranged vessels after transplantation in mice. Gene-gene interaction networks and regulatory effects identified by IPA revealed the disease mechanism in a transcriptional level. A clear overview of the complex interactions among dysregulated genes caused by *SERPINE1-FOSB* translocation, as well as cellular functions and activities that were affected by these dysregulated genes were obtained in this part of the study. Notably, angiogenesis, vascularization and tumor-related process were activated/promoted by these dysregulated genes in hiPSC-EC$^{SERPINE1\text{-}FOSB}$. This explained pathologies of PHE tumor development at the transcriptional level: the driver *SERPINE1-FOSB* mutation caused downstream dysregulated genes in hiPSC-EC$^{SERPINE1\text{-}FOSB}$ which further lead to aberrant cellular function and activities in ECs. Compared to the interaction map included in the main Chapter (**chapter 6**), the interaction map drawn in this appendix provided new information about the gene-gene interactions and thus new insights into the disease mechanisms of PHE. Most importantly, two candidate drugs which could target on a large number of dysregulated genes in hiPSC-EC$^{SERPINE1\text{-}FOSB}$ were also identified in this appendix. Especially, drug PD98059 was predicted as able to have an inhibitory effect on both *SERPINE1* and *FOSB* expression. We conclude it could be a potential drug for PHE, which should be further tested both *in vitro* and *in vivo* in the future.

In summary, these extra bioinformatic analyses of PHE hiPSC model provided extra key insights about disease mechanisms of PHE and identified two candidate drugs for the treatment of the disease. The analysis here was not only complementary to the

analysis in the main chapter, but also presented important new information about the disease.

METHODS

*Methods of this chapter appendix only cover the methods that are specific to this appendix which were not included in the main chapter (**Chapter 6**).*

Principle component analysis (PCA) and HCA

PCA plot was generated with the built-in R functions prcomp using transposed normalized RPKM matrix.

Ingenuity pathway analysis (IPA)

Interaction networks among input genes were generated using Interaction network analysis function of IPA software. Map of genes in specific cellular positions was generated with build-in **layout** option of IPA software. Upstream regulators and downstream functions/activities of input genes were identified with build-in **Regulatory effects** function of IPA. Candidate drugs that target on a list of input genes were identified using a build-in **Drug prediction** function of IPA.

REFERENCES

Hornick, J.L., and Fletcher, C.D. (2011). Pseudomyogenic Hemangioendothelioma. Am J Surg Pathology *35*, 190–201. WT.